Investigation of Polypropylene Glycol 425 as Possible Draw Solution for Forward Osmosis

Mads Koustrup Jørgensen

Master Thesis

June 2009

Department of Chemistry, Biotechnology and Environmental Engineering

Aalborg University

The Faculties of Engineering, Science and Medicine
Aalborg University

Department of Biotechnology, Chemistry and Environmental Engineering

Investigation of Polypropylene Glycol 425 as a Draw Solution for Forward Osmosis

M.Sc. Thesis:
9th & 10th semester,
September 1st, 2008 -
June 4th, 2009

Student:
Mads Koustrup Jørgensen

Supervisor:
Kristian Keiding

Danish title:

Undersøgelse af Polypropylen Glycol 425 som Trækkende Opløsning til Direkte Osmose

Editions: 5

Pages: 69

Appendices: 1 + CD-rom

Mads Koustrup Jørgensen

Abstract:

In this Master Thesis, Polypropylene Glycol 425 (PPG) is studied as a potential draw solution for forward osmosis. The requirements of an effective draw solution is a high osmotic pressure for high flux, low concentration polarization and that it can be regenerated effectively to reclaim the water drawn from the feed solution.
Therefore the osmotic pressure of PPG solutions at different concentrations and temperatures is described. For this purpose water activity of different concentrations PPG is measured at different temperatures. These data is described with the van't Hoff equation.
The water activities show high osmotic pressures at 15 ^{o}C and high concentrations. At higher temperatures, the solubility of PPG decreased and at 50 ^{o}C the solutions phase separates.
Using this knowledge, forward osmosis has been performed at 15 ^{o}C, using PPG draw solution and NaCl feed solutions of different concentrations. The experimental flux, compared to theoretical flux, is reduced by concentration polarization. Modeling the flux show some consistency with measured flux at different concentrations of feed solution, but not draw solution.
The separation of PPG solutions was not effective. High M_w polymers precipitated at 50 ^{o}C, but at 80 ^{o}C, 60 to 74 % of the low M_w polymers were still in solution. A more monodisperse solution might give a better separation.
It is concluded, that PPG solutions has osmotic pressures to create flux from NaCl feed solutions. However, the separation of the PPG solutions was not efficient for regeneration of draw.

Dansk resumé

I dette speciale undersøges det, hvorvidt Polypropylen Glycol 425 (PPG) kan anvendes som trækkende opløsning i direkte osmose. Kravene til en effektiv trækkende opløsning er at der skal være højt osmotisk tryk for at skabe en høj flux af vand, lav koncentrationspolarisering samt at den trækkende opløsning effektivt kan regenereres, således at vandet, der trukket fra fødestrømmen, igen kan frigives.
Derfor beskrives det osmotiske tryk af PPG-opløsninger ved forskellige koncentrationer temperaturer. Til dette formål måles vandaktiviteten af PPG-opløsninger, med forskellige koncentrationer til forskellige temperaturer. Disse data beskrives med van't Hoff ligningen.
Vandaktiviteten viser højt osmotisk tryk ved 15 ^{o}C og høje koncentrationer. Ved højere temperaturer nedsættes PPG's opløselighed og ved 50 ^{o}C adskilles de i to faser.
Ud fra dette er direkte osmose udført ved 15 ^{o}C, med forskellige koncentrationer af både PPG-opløsninger og NaCl-opløsninger. PPG-opløsningerne er anvendt som trækkende opløsninger, mens NaCl-opløsninger er anvendt i fødestrømmen. Den eksperimentelle flux af vand er, sammenlignet med den teoretiske flux, nedsat af koncentrationspolarisering. Modellering af fluxen stemmer nogenlunde overens med de forskellige fødestrømskoncentrationer, mens de trækkende opløsningers koncentrationer ikke har vist nogen klar sammenhæng med modellen.
Separationen af PPG-opløsninger i dette projekt er ineffektiv. De lange PPG-polymerkæder udfældede ved 50 ^{o}C, mens der ved 80 ^{o}C stadig var opløst 60-74 % af de kortere PPG-polymerkæder. En mere monodispers størrelsesfordeling af PPG-kæder vil muligvis give en bedre separation.
Det er konkluderet at PPG-opløsninger har osmostisk tryk nok til at skabe en flux fra fødestrømmen indeholdende NaCl. Dog er frigivelsen af vandet ikke effektiv.

Preface

This Master Thesis is completed at Aalborg University as a final part of the education for Master of Science in Engineering, Chemistry.
References are stated in square brackets, i.e. [Author, year of publication], and can be found in the Bibliography. References are done according to the Harvard method.
A list over the nomenclature is placed before the bibliography.
The enclosed CD contains the thesis, articles, raw data and processed data.

I would like to acknowledge:

- Associate Professor Søren Hvidt, Roskilde University, for guiding me on PPG related topics.
- Research Manager Ebbe Kruse Vestergaard, Grundfos Management A/S, for inspiration and guidance.
- Associate Professor Kristian Keiding, not for the supervision but for his extraordinary interest and support.
- My fellow students for their interest in my project, help and the forum of discussing issues of the thesis.
- Maria Sigsgaard for her great help and support during the project.

Contents

1. Introduction

1.1 Water treatment in the future

The demand of fresh water today is critical. 1.2 billion people have no access to fresh drinking water and 2.6 billion people do not have sanitation [Shannon et al., 2008]. The lack of fresh water causes diseases to spread and kill millions of people every year. Furthermore the water consumption and the amount of waste water are increasing [Shannon et al., 2008]. Therefore, it is relevant to investigate how to obviate the world's growing water consumption and need for purification of water [Shannon et al., 2008].
Conventional methods for water purification can solve some of the problems regarding disinfection and desalination. Though, the already known methods demand much energy and infrastructure, and thus they are too expensive for the developing countries, that causes a major part of the growing demand of water [Shannon et al., 2008].
Therefore, it is necessary to develop new methods for water treatment. The current developments of water purification includes disinfection of water without use of chemicals, removing contaminants at low concentrations, purification of waste water and desalination of sea water for drinking water [Shannon et al., 2008]. For these purposes, membrane filtration has proved efficient and has a high potential for further development. In the case of waste water treatment, Membrane Bioreactors (MBR) is a promising technology combining suspended growth bioreactor with micro- or ultrafiltration [Bixio et al., 2006]. The MBR's are ideal for decentralized sewage treatment in the developing countries because they do not take up much space and the design is flexible [Shannon et al., 2008]. For further treatment of the effluent, reverse osmosis (RO) can remove the remaining salts of the effluent, producing potable drinking water [Shannon et al., 2008].
RO is also used for desalination [Schiermeier, 2008]. In a number of countries, the technology does already produce fresh water from seawater. There are two problems using RO. First, a high pressure is required and thus high-cost electrical energy [Shannon et al., 2008]. Second, fouling of the membranes reduces the flux and makes it necessary to frequently replace membranes [Schiermeier, 2008].
A new method for desalination, forward osmosis (FO) or direct osmosis, is under investigation [Shannon et al., 2008]. Since the process, when compared to RO, is not pressure driven there is a lower fouling propensity [Cath et al., 2006]. Also, the use of low grade energy instead of electrical energy makes FO more favorable [Shannon et al., 2008]. Another advantage for food or pharmaceutical processing is that the process neither demands high temperature, that as well as high pressure, could be detrimental to the feed solution [Cath et al., 2006].

1.2 Forward Osmosis

When having two solutions of different osmotic pressure separated by a semi-permeable membrane, the difference a flux of water from the low osmotic solution arises toward the higher osmotic solution [Atkins and de Paula, 2002]. From this principle, the terms reverse and forward osmosis occurs, illustrated in figure 1.1 [Lee et al., 1981].

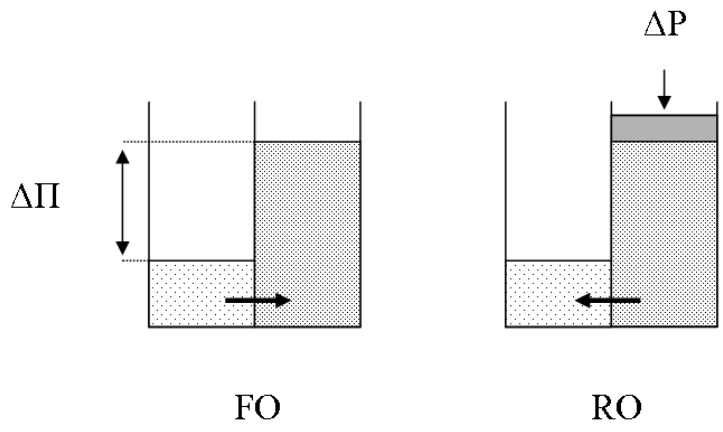

Figure 1.1: Illustration of FO and RO. Inspired by Cath et al. (2006)

Reverse osmosis is the process of an osmotic feed solution being applied a pressure, ΔP, to exceed the difference in osmotic pressure between the feed and permeate solution [Lee et al., 1981]. Then a flux of water, J_w, from feed to permeate solution arises, described by equation 1.1.

$$J_w = A\left((\Pi_F - \Pi_P) - \Delta P\right) \tag{1.1}$$

Where A is the water permeability constant of the membrane, Π_F and Π_P is osmotic pressure of feed and permeate solution respectively, and ΔP is the difference in applied pressure [Lee et al., 1981].
The rejection, $r_{rejection}$ describes the relative amount of solute rejected [Lee et al., 1981]:

$$r_{rejection} = 1 - \frac{C_P}{C_F} \tag{1.2}$$

Where C_P is the concentration of feed solute in permeate and C_F is the concentration of feed. I.e. a rejection of 1 or 100 % is a total rejection of feed solutes.
In forward osmosis, the permeate solution is named the draw solution and [Cath et al., 2006]. The draw solution contains solutes that gives an osmotic pressure higher than the the feed solution. Because of this difference in osmotic pressure, an osmotic gradient will create a flux of water through the membrane to the draw solution

as illustrated in figure 1.1 on the preceding page [Lee et al., 1981]. Thus, the applied pressure given in equation 1.1 equals zero in FO:

$$J_w = A\left(\Pi_D - \Pi_F\right) \tag{1.3}$$

The next step in the FO filtration process is to regenerate the draw solution [Cath et al., 2006]. I.e. when the draw solution is diluted, it has to be reconcentrated in order to maintain a high flux and to release the water from the feed solution. This step is the main energy consuming part of the FO process [McGinnis and Elimelech, 2007].
There are two advantages using FO instead of RO. First, the fouling of the membranes are lower, because the driving force is a difference in concentration instead of a hydraulic pressure [Holloway et al., 2007]. Second, it is less energy consuming if a suitable draw solution is found, i.e. the energy for regeneration of draw solution is lower than the energy of creating the hydraulic pressure required for RO [McGinnis and Elimelech, 2007]. Even though FO has advantages, the flux of water is often lower than expected as a cause of concentration polarization [Lee et al., 1981, McCutcheon et al., 2006].
Therefore, there are two concerns regarding FO: First, to be able to describe the flux of water, taking concentration polarization into account. Second, to select an effective draw solution regarding both high flux, i.e. high osmotic pressure, and low energy of regeneration [Cath et al., 2006].

1.3 Concentration Polarization

Concentration polarization (CP) occurs as a lower flux than expected is measured. It can be expressed by the performance ratio, $r_{performance}$ [Cath et al., 2006]:

$$r_{performance} = \frac{J_{w,experimental}}{J_{w,theoretical}} \cdot 100\% \tag{1.4}$$

Where $J_{w,experimental}$ is the measured flux and $J_{w,theoretical}$ is the flux estimated from equation 1.3. The performance ratio does, however, not fully describe the CP, as both external concentration polarization (ECP) and internal concentration polarization (ICP) occurs [McCutcheon and Elimelech, 2006].
The phenomena of ECP is illustrated in figure 1.2 on the following page.

The figure shows the concentration profile of osmotic substances along a membrane As water diffuse from the feed solution into the membrane, a local concentration of the feed occurs [McCutcheon and Elimelech, 2006]. At the draw side of the membrane, a local dilution occurs when water from the membrane diffuse into the solution

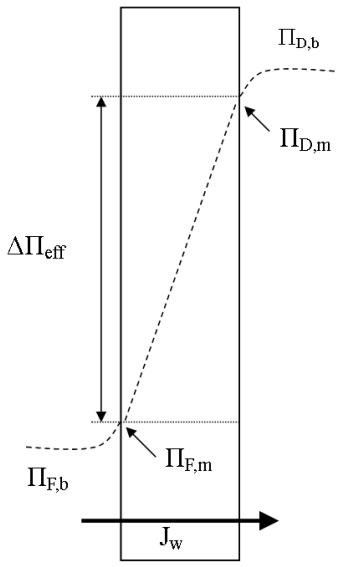

Figure 1.2: External concentration polarization. The line is the concentration profile, indicating concentrative ECP (right) and dilutive ECP (left).

[McCutcheon and Elimelech, 2006]. This causes external concentration polarization in a boundary layer against the membrane, reducing the effective osmotic gradient.
In the following mass balance, the ECP at the feed side of the membrane is described [Clement et al., 2004].

$$J_w C = J_w C_d - D\frac{dC}{dx} \tag{1.5}$$

C is the concentration of solute in the layer at length x from the membrane, C_d is the concentration of draw, D is the diffusion coefficient of solute and $\frac{dC}{dx}$ is the concentration gradient within the boundary layer. Using the boundary conditions, $C = C_{membrane}$ when $x = 0$ and $C = C_{bulk}$ when x =layer thickness, δ and presuming total rejection of salt, the following equation is obtained [Clement et al., 2004]:

$$\frac{C_{membrane}}{C_{bulk}} = exp\left(\frac{J_w \delta}{D}\right) \tag{1.6}$$

This relationship is called the polarization modulus. This can be concentrative or dilutive, dependent on whether it is the feed or draw ECP studied. In case of dilutive ECP, the exponential term will be negative.
δ/D can be replaced with the mass transfer coefficient k_D and k_F for ECP in draw and feed respectively.
McCutcheon and Elimelech (2006) describes the mass transfer coefficient, k, as equation 1.7:

$$k = \frac{ShD}{d_h} \tag{1.7}$$

Where Sh is the Sherwood number and d_h the hydraulic diameter. The mass transfer coefficient for NaCl at 20 °C and a crossflow velocity of 21.4 cm/s has been determined to 62.6 $\frac{L}{h \cdot m^2}$ [McCutcheon and Elimelech, 2007]. As osmotic pressure is a colligative property, the polarization modulus is also expressed as the relationship [McCutcheon and Elimelech, 2006]:

$$\frac{\Pi_{membrane}}{\Pi_{bulk}} = exp\left(\frac{J_w}{k}\right) \tag{1.8}$$

Where $\Pi_{membrane}$ is the osmotic pressure at the membrane and Π_{bulk} is the osmotic pressure in bulk.
According to Clement et. al. (2004) the polarization modulus increases with:

- Increasing flux, J_w
- Thickness of boundary layer, δ
- Lower diffusion coefficient, D

The thickness of the boundary layer can be reduced with higher crossflow or lower viscosity, and the diffusion coefficient depends on both temperature and solute [Clement et al., 2004].
Combining equation 1.6 with equation 1.1 an expression for J_w as a function of Π_D and Π_F with respect to ECP is obtained:

$$J_w = A\left(\Pi_D exp\left(\frac{-J_w}{k_D}\right) - \Pi_F exp\left(\frac{J_w}{k_F}\right)\right) \tag{1.9}$$

Though, equation 1.9 does not describe the internal concentration polarization (ICP). RO membranes usually consist of a thick porous layer, supporting the active rejecting layer. ICP occurs in the membrane support layer, as water diffuse through the membrane, resulting in an dilution or concentration of solutes, as illustrated in figure 1.3 on the next page [Gray et al., 2006].

The figure shows two FO membranes oriented different to the draw and feed solutions and the concentration profile of osmotic substances in the feed and draw solutions and through the membranes supporting layer.
When the membrane support layer is placed toward the draw solution, dilutive ICP occurs as solute in the membrane is diluted [Gray et al., 2006]. If the membrane support layer is placed against the feed solution, the feed solute in the support layer is concentrated as water diffuse through the membrane [Gray et al., 2006]. This is called concentrative ICP. The extent of the ICP depends on the solute resistance to diffusion in the membrane

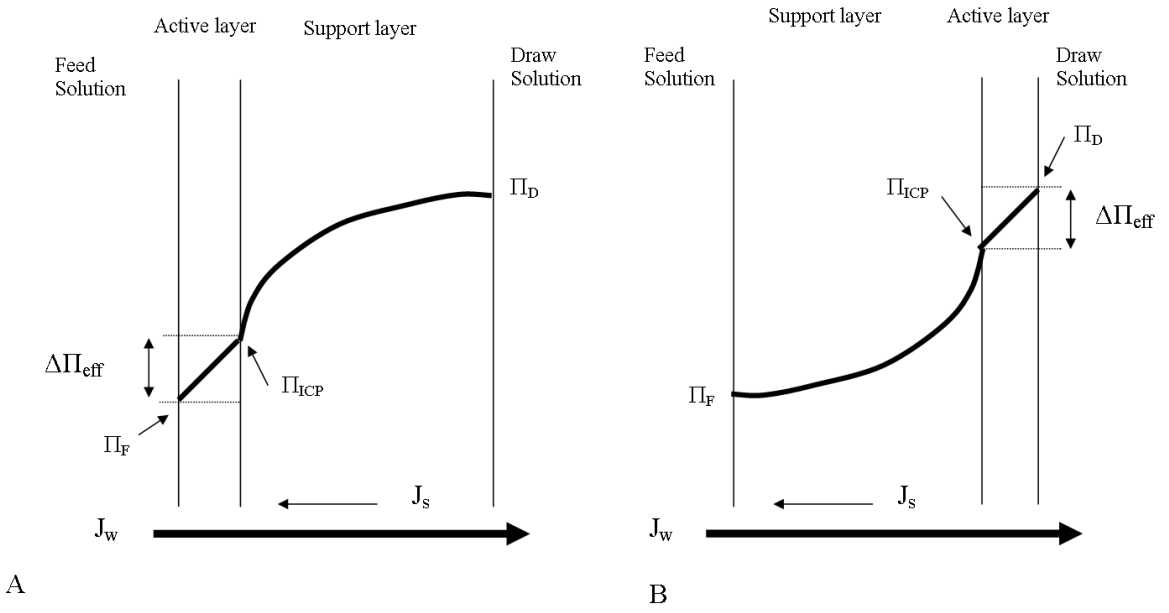

Figure 1.3: (A) Dilutive internal concentration polarization and (B) concentrative internal concentration polarization

support layer, K. This is presented by Lee et. al. (1981):

$$K = \frac{t\tau}{D\epsilon} \tag{1.10}$$

t, τ and ϵ is the thickness, tortuosity and porosity of the support layer, and D is the bulk diffusion coefficient of the solute. Because the solute resistance to diffusion depends on the membrane thickness, special FO membranes have been developed by Hydration Technologies, Inc [McCutcheon et al., 2006]. The cellulose triacetate (CTA) membranes thickness is reduced embedding a polyester mesh for extra support [McCutcheon et al., 2006]. Using the CTA membrane instead of a conventional RO membrane reduces the membrane thickness from 140 μm to under 50 μm, and the flux increases significantly [McCutcheon et al., 2006]. The membrane permeability is measured to 1.12 $\frac{L}{atm \cdot h \cdot m^2}$ by measuring the permeate flux at different pressures of water [McCutcheon et al., 2005].
As seen in equation 1.10, the solute resistance also depends on the solute diffusion coefficient. This means, that higher diffusion of solute leads to better compensation for the dilutive or concentrative ICP respectively, as illustrated in figure 1.3 [McCutcheon et al., 2006]. Therefore, to obtain the lowest solute resistance, the membrane support layer has to be next to the solution of solutes with the highest diffusion coefficient. Though, the support layer is more exposed to fouling than the rejection layer [Mi and Elimelech, 2008]. For NaCl solutions at 20 °C K is lower for concentrative ICP, 16.1 $\frac{h \cdot m^2}{L}$, than dilutive ICP, 13.5 $\cdot 10^{11}$ [Mi and Elimelech, 2008].
The solute resistance to diffusion, K, can be incorporated into equation 1.9 in two ways [McCutcheon and Elimelech, 2006]. Equation 1.11 describes the flux with dilutive ICP

[McCutcheon and Elimelech, 2006]:

$$J_w = A\left(\Pi_D exp\left(\frac{-J_w K}{k_D}\right) - \Pi_F exp\left(\frac{J_w}{k_F}\right)\right) \tag{1.11}$$

With concentrative ICP, the expression is written [McCutcheon and Elimelech, 2006]:

$$J_w = A\left(\Pi_D exp\left(\frac{-J_w}{k_D}\right) - \Pi_F exp\left(\frac{J_w K}{k_F}\right)\right) \tag{1.12}$$

For simplicity, equation 1.12 is in this thesis rewritten

$$J_w = A\left(\Pi_D exp\left(\frac{-J_w}{k_D}\right) - \Pi_F exp\left(\frac{J_w}{k_{CP,F}}\right)\right) \tag{1.13}$$

where $k_{CP,F} = k_F/K$.
From equation 1.13 it is given, that lowering Π_F gives a higher flux. The higher flux will give an exponential increase in polarization modulus. The modulus for the draw solution will on the contrary decrease at higher fluxes. This gives the concentration of feed and dilution of draw, lowering the effective osmotic gradient. Therefore, the flux of water can be modeled using the given expressions for FO with different membranes, draw and feed solutions.

1.4 Draw Solutions and Applications of Forward Osmosis

Waste water treatment
FO has been tested as a pre-treatment step in wastewater treatment to reduce fouling problems for concentration of various types of waste water. Various processes have been examined, all with the common feature, that the draw solution was a 7-7.5 % NaCl solution. The draw solution was reconcentrated with RO.
The applications tested are, among others, concentration of digester centrate, and reclamation of waste water in space missions [Holloway et al., 2007, Cath et al., 2005]. The tests showed effective flux, but rejection of ammonia from digester centrate and urea respectively was low. The specific power consumption was between 15 and 30 kWh/m^3 for the NASA and Osmotek test unit of wastewater reclamation in space [Cath et al., 2005]. For leachate treatment, a full-scale treatment plant has been constructed in Oregon, USA [York et al., 1999]. Between June 1998 and March, 1999, it treated over 18,500 m^3 leachate with an average recovery of 91.9 % and a rejection of most pollutants at 99 % [York et al., 1999].
Food processing

FO has also been tested for use as pretreatment for food processing because of the low fouling potential compared to RO. Petrotros et al. (1998) studied concentration of tomato juices with solutions of sodium chloride, calcium chloride, calcium nitrate, glucose, sucrose and Polyethylene Glycol (PEG) 400. They concluded that the best flux of water was obtained with the salt solutions, because the flux of the carbohydrate and PEG solutions were much lower than expected [Petrotos et al., 1999].

Desalination of seawater

For desalination of seawater, the development of draw solutions is the major development that has been investigated. Batchelder (1965) suggested a FO process for desalination of seawater with removal of the draw solute, by dissolving volatile solutes like sulfur dioxide in water for draw solution. The solution created a flux of water over an cellulosic membrane from seawater [Batchelder, 1965]. When the solution is diluted, the volatile osmotic agent is removed by heating.

In the same way, Glew (1965) suggests that either gases or liquids are used as osmotic solutes for draw solutions. The technique developed uses solutions of sulfur dioxide or aliphatic alcohols creating a sufficient osmotic pressure for desalination of seawater [Glew, 1965]. In contrast to Batchelder (1965) reuse instead of removal of draw solute is suggested [Glew, 1965].

Aluminum sulfate dissolved in water has been studied as draw solution for desalination of seawater [Frank, 1972]. The aluminum sulfate is precipitated when adding calcium hydroxide [Frank, 1972]. Though, in this method it is not possible to reuse the precipitated osmotic agent.

Solutions of carbohydrates have also been proposed for draw solutions for desalination. Kravath (1975) creates a flux of water from seawater to a concentrated glucose solution in a dialysis cell. The possible use of this cell is in emergency lifeboats where a dialysis bag can be emerged into the seawater. A flux from seawater over a cellulose acetate membrane dilutes the salt/glucose solution to a level where ingestion is possible [Kravath and Davis, 1975]. Though the osmotic agent is consumed, the method does not demand removal of the osmotic agent. Therefore, this method is not suited for large scale water treatment for potable water.

For now, the most developed and energy effective FO process for desalination is based on using a ammonia-carbon dioxide draw solution, as illustrated in figure 1.4 on the next page [McCutcheon et al., 2006, McGinnis and Elimelech, 2007].

As fresh water is drawn from the saline water into the draw solution, the draw solution is diluted, lowering the osmotic pressure. The diluted draw solution is recovered in the recovery system, where the filtrated water is to be separated from the draw solution to obtain purified water. The ammonium salts in the draw solution decompose to NH3 and CO_2 gases when heated to 60 °C [McCutcheon et al., 2006]. When the osmotic agent is separated from the water, the purified water is obtained. The last step is the full recovery

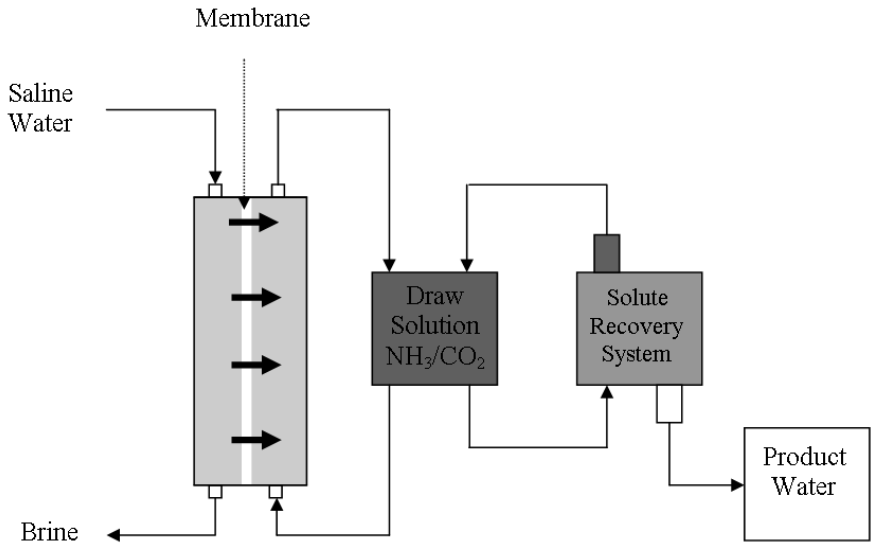

Figure 1.4: Schematic presentation of the ammonia-carbon dioxide FO desalination process from McGinnis and Elimelech (2007).

of the draw solution, by condensing the gases to dissolve them in water and form the salt solutions again [McCutcheon et al., 2006].
If a single vacuum distillation column is used as a recovery system, the temperature for recovery of draw can be reduced to 40 °C in a reboiler [McGinnis and Elimelech, 2007]. It induces water vapor to rise upwards the distillation column as the diluted draw flows down through the column [McGinnis and Elimelech, 2007]. Energy transfer between the counter current flow of steam and diluted draw causes fractional separation of the less volatile ammonia and carbon dioxide [McGinnis and Elimelech, 2007]. Therefore, the amount of ammonia and carbon dioxide in the steam is higher in the top of the column, than at points lower in the column. At the vacuum level at the top of the column, the gases from the stream are condensed with air, recovering the draw solution.
The energy required for this recovery of ammonia-carbon dioxide draw is primarily thermal but also electrical energy for fluid pumping is needed [McGinnis and Elimelech, 2007]. McGinnis and Elimelech (2007) compared the energy for desalination of seawater with ammonia-carbon dioxide FO and RO filtration. The equivalent work for desalination with a 1.5 M ammonium-carbon dioxide draw, cellulose triacetate membrane and single vacuum distillation column for recovery was 0.84 kWh/m^3. Desalination with RO has a equivalent work at 3.02 kWh/m^3. Therefore, FO desalination was concluded less energy consuming for desalination than RO [McGinnis and Elimelech, 2007].
Using a 1.6 M ammonium-carbon dioxide draw and 0.5 M , 2.9 %, NaCl feed the difference in osmotic pressure is 48.4 atm [McCutcheon et al., 2006]. From this, a flux of 10.08 $\frac{L}{h \cdot m^2}$ has been obtained, corresponding to a performance ratio of 10.2 %. For NaCl concentrations 0.05 to 2 M and ammonium-carbon dioxide draw concentrations fluxes between 3.24

and 36.4 $\frac{L}{h \cdot m^2}$ was measured with performance ratios in the range 2.4 to 20.4 % with an average of 5 - 10 % [McCutcheon et al., 2006].
Therefore, the ammonia carbonate FO system has high fluxes and can be regenerated. Though a problem with the draw solution is the high pH, damaging the membrane [McGinnis and Elimelech, 2007].
To further develop FO suited for large scale effective water treatment, it is still important to discover new possible draw solutions for FO and develop membranes.
PEG solutions has proved to create a flux of water in FO with tomato juice [Petrotos et al., 1999]. However, PEG - water solutions can not be thermally separated for regeneration [Kirk, 1966]. Polypropylene Glycol (PPG) though, is hydrophilic at room temperatures, and hydrophobic at higher temperatures [Kirk, 1966]. PPGs with molecular weights below 500-550 g/mol are fully miscible with water, but above this, the solubility decreases rapidly [Kirk, 1966]. Though, they are less hygroscopic than PEG solutions, and thus, have less osmotic pressure and lower driving force for forward osmosis. Therefore, low molecular weight PPG solutions might be reconcentrated and might be possible draw solutions for FO, depending on:

- The osmotic pressure of PPG solutions at different temperature and concentration
- The degree of concentration polarization in FO
- The energy required for regeneration

1.5 Thesis Statement

The aim of this thesis is to investigate the potential of polymeric draw solutions for forward osmosis by answering the following question:

Can Polypropylene Glycol solutions create a flux from sodium chloride solutions and be separated for regeneration, as a possible draw solution for forward osmosis?

This will be answered by characterizing:

- The temperature and concentration dependence of the osmotic pressure of Polypropylene Glycol solutions
- Modeling the flux obtained when using a Polypropylene Glycol draw solution and a sodium chloride feed solution
- The separation of Polypropylene Glycol solutions for regeneration

In the study of flux, NaCl solutions are chosen as feed solutions, as they have a well defined osmotic pressure.

2. Theory

2.1 Osmotic Pressure and Water Activity

The osmotic pressure is described by the water activity [Atkins and de Paula, 2002]. The following figure 2.1 shows a solution and a solvent separated by a semi-permeable membrane. From this, osmotic pressure can be defined from water activity [Atkins and de Paula, 2002].

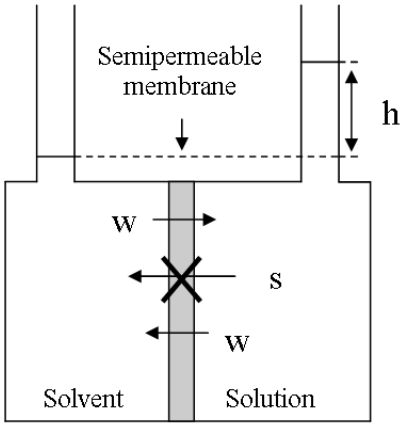

Figure 2.1: A solvent, left, and solution, right, separated by a semi-permeable membrane. Inspired from Atkins and de Paula (2002)

The difference in height observed, h, relates to the osmotic pressure. The chemical potential of water, μ_w in the solution can be expressed as follows [Hiemenz and Rajagopalan, 1997]:

$$\mu_w = \mu_w^0 + RTln(a_w) \tag{2.1}$$

Where R is the gas constant, T is the absolute temperature in Kelvin, μ_w^0 is the standard chemical potential of water and a_w the water activity. At the right side of the membrane, the chemical potential of water equals μ_w^0, as no solute is present. Because a_w of the solution equals 1, the chemical potential of the solution is lower than the potential of the solvent. This causes more than average solvent molecules to diffuse from the solvent to the solution. Equilibrium is obtained when the difference in height between solvent and solution, h, counteracts the $RTln(a_w)$ term in equation 2.1 [Hiemenz and Rajagopalan, 1997]. From the expression $\left(\frac{\delta G}{\delta P}\right)_T = V$, the pressure dependence of chemical potential of the so-

lution can be expressed [Hiemenz and Rajagopalan, 1997]:

$$\left(\frac{\Delta\mu_w}{\Delta P}\right)_T = \bar{V}_w \tag{2.2}$$

Where $\bar{V}_w$ is the partial molar volume of water. Integrating equation 2.2 leads to an expression of the osmotic pressure required to counterbalance the difference in chemical potential of water, $\Delta\mu_w$ [Hiemenz and Rajagopalan, 1997]:

$$\Delta\mu_w = \int_P^{P+\Pi} \bar{V}_w dP = \bar{V}_w \Pi \tag{2.3}$$

Where P is the external atmospheric pressure. According to equation 2.1 and 2.3, equilibrium is obtained, i.e. $\mu_w^0 = \mu_w$, water activity is [Atkins and de Paula, 2002]:

$$\mu_w = \mu_w^0 + RTln(a_w) + \bar{V}_w \Pi \tag{2.4}$$

This leads to the osmotic pressure:

$$\Pi = -\frac{RT}{\bar{V}_w} ln(a_w) \tag{2.5}$$

Thus, measuring the water activity, the osmotic pressure of the solution can be determined. Water activity can be measured by, e.g. from the dew point technique, based on the Clausius-Clapeyron equation 2.6 [Devagon Devices, udat]. In this method, the dew point of water on e.g. a chilled mirror over a sample is detected.

$$p_w^T = p_w^{T^0} \cdot exp\left(\frac{-\Delta H_{vap}}{R}\left(\frac{1}{T} - \frac{1}{T^0}\right)\right) \tag{2.6}$$

T^0 is the dew point temperature, p_w^T is the water vapor pressure at temperature T, and $p_w^{T^0}$ the vapor pressure at dew point.
From the vapor pressure determined in equation 2.6, the water activity can be determined [Atkins and de Paula, 2002]:

$$a_w = \frac{p_w}{p_w^0} \tag{2.7}$$

Where p_w^0 is the saturated water vapor pressure. Osmometric determination of water activity can be carried out by Peltier-cooling a mirror or thermocouple below the dew point, and detect the dew point temperature.
As the mole fraction of water, x_w, equals the water activity for an ideal solution, the osmotic pressure can be expressed with the concentration by rewriting equation 2.5 [Hiemenz and Rajagopalan, 1997]:

$$\Pi = -\frac{RT}{\bar{V}_w} ln(x_w) = -\frac{RT}{\bar{V}_w} ln(1 - x_s) \tag{2.8}$$

Where x_w and x_s are the mole fraction of water and solute respectively.
For low concentrations $x_s \approx \frac{n_s}{n_w}$ and as $ln(1-x_s) = -x_s - \frac{x_s^2}{2} - ...$, equation 2.8 can be written for infinite dilution, tending toward ideality [Hiemenz and Rajagopalan, 1997]:

$$\frac{n_s}{n_w} = \frac{\Pi \bar{V}_w}{RT} \tag{2.9}$$

From this, the osmotic pressure as a function of concentration of ideal solution is expressed:

$$\Pi = \frac{n_s}{n_w}\frac{RT}{\bar{V}_w} = c_s RT \tag{2.10}$$

Though, the use of equation 2.10 is limited to ideal solutions. To describe the osmotic pressure of a real solution, equation 2.5 is rearranged:

$$-\frac{\Pi \bar{V}_w}{RT} = ln(a_w) = ln(1-a_s) = -a_s - \frac{a_s^2}{2} - ... \Updownarrow \frac{\Pi \bar{V}_w}{RT} = a_s + \frac{a_s^2}{2} + ... \tag{2.11}$$

To describe the non-ideality of gases, a virial expression is used in the ideal gas law [Hiemenz and Rajagopalan, 1997]:

$$\frac{pV}{nRT} = 1 + B\left(\frac{n}{V}\right) + C\left(\frac{n}{V}\right)^2 + ... \tag{2.12}$$

Where B and C are virial coefficients, describing deviations from ideality. Since the relationship of osmotic pressure of a solution and pressure of a gas are described in the same manner with 2.9 and the ideal gas law respectively, the virial coefficients are introduced in equation 2.11, to substitute a_s with x_s [Hiemenz and Rajagopalan, 1997].

$$\frac{\Pi \bar{V}_w}{RT} = x_s + B\frac{x_s^2}{2} + ... \tag{2.13}$$

The mass concentration is expressed:

$$c = \frac{m_s}{n_w \bar{V}_w + n_s \bar{V}_s} = \frac{m_s}{n_w \bar{V}_w} \tag{2.14}$$

Where m_s is the mass of solute. This expression is only valid at $n_s << n_w$ [Hiemenz and Rajagopalan, 1997]. From equation 2.14:

$$c = \frac{n_s M_s}{n_w \bar{V}_w} = x_s \frac{M_s}{\bar{V}_w} \tag{2.15}$$

Combining equation 2.13 and equation 2.15 gives the osmotic pressure dependence of concentration:

$$\frac{\Pi \bar{V}_w}{RT} = \frac{\bar{V}_w}{M_s}c + \frac{1}{2}B\left(\frac{\bar{V}_w}{M_s}\right)^2 c^2 + ... \tag{2.16}$$

Neglecting higher orders of non-ideality, equation 2.17 is rearranged:

$$\frac{\Pi}{RTc} = \frac{1}{M_s} + \frac{1}{2}\frac{B\bar{V}_w}{M_s^2}c \tag{2.17}$$

Therefore, plotting the reduced osmotic pressure, $\frac{\Pi}{RTc}$, versus c gives a straight line, if the higher order deviations from ideality can be neglected. The inverse of the intercept is the molar mass of the solute. This is a common osmometric determination of polymers molecular weight [Hiemenz and Rajagopalan, 1997]. The slope relates to the first second virial coefficient, B. It can be modified to B'=$\frac{1}{2}\frac{B\bar{V}_w}{M_s^2}$, that has the same properties as B. For ideal solutions, B' equals unity [Hiemenz and Rajagopalan, 1997].

2.2 BET Isotherm for Dependence of Concentration

The BET isotherm is originally an adsorption isotherm, describing the adsorption of water vapor on a surface from the water activity by equation 2.18 [Atkins and de Paula, 2002].

$$Y = \frac{Y_{mono} \cdot j \cdot a_w}{(1 - a_w)\,(1 - (1 - ja_w))} \tag{2.18}$$

where Y is the water content in g_w/g_s, Y_mono is the water content at the surface of the adsorbing layer and j is a constant, that can relate to the excess enthalpy by the following equation [Atkins and de Paula, 2002]:

$$j = exp\left(\frac{-\Delta H^0_{excess}}{RT}\right) \tag{2.19}$$

For simplicity, the BET isotherm can be linearized by equation 2.20 [Atkins and de Paula, 2002].

$$\frac{a_w}{(1 - a_w)\,Y} = \frac{1}{jY_{mono}} + \frac{(j-1)\,a_w}{jY_{mono}} \tag{2.20}$$

As stated before, the isotherm describes the equilibrium of water adsorbed to a surface:

$$H_2O\,(g) \rightleftharpoons H_2O\,(ads)$$

Where $H_2O\,(ads)$ is water vapor adsorbed to the surface. But, the equilibrium of water adsorbed to or arranged with a solute in solution can be described:

$$H_2O\,(g) \rightleftharpoons H_2O\,(l) \rightleftharpoons H_2O\,(bound)$$

Where $H_2O\,(l)$ is water in solution and $H_2O\,(bound)$ is water arranged with the solute. Therefore, assuming that water is adsorbed in the same way as it is adsorbed to a surface,

the BET isotherm can be used to describe the water activities of solutions at different concentrations.

2.3 Describing Temperature Dependence by van't Hoff Equation

To describe the temperature dependency of the water activity, and thereby osmotic pressure, the van't Hoff equation is derived. The isosteric enthalpy of adsorption is the extra enthalpy of condensing water to a surface relative to the enthalpy of condensation [Atkins and de Paula, 2002]. It can be described from the following expression, deriving the van't Hoff equation:

$$\frac{\delta ln(K_{eq})}{\delta T} = \frac{\Delta H^0_{adsorption}}{RT^2} \tag{2.21}$$

Where K_{eq} is the equilibrium constant. Next, it is rewritten:

$$\int_{Tref}^{T} dln(K_{eq}) = \int_{Tref}^{T} \frac{-\Delta H^0_{adsorption}}{RT^2} dT \tag{2.22}$$

Integrating this equation gives [Atkins and de Paula, 2002]:

$$ln\left(\frac{K_{eq}(T)}{K_{eq}(T_{ref})}\right) = -\frac{\Delta H^0_{adsorption}}{R}\left(\frac{1}{T} - \frac{1}{T_{ref}}\right) \tag{2.23}$$

From equation 2.23 the following expression is:

$$K_{eq}(T) = K_{eq}(T_{ref}) exp\left(\frac{-\Delta H^0_{adsorption}}{R}\left(\frac{1}{T} - \frac{1}{T_{ref}}\right)\right) \tag{2.24}$$

Using $ln(K) = -\frac{\Delta G^0}{RT}$ and $\Delta G^0 = \Delta H^0 - T \cdot \Delta S^0$ and setting $T = T_{ref}$, equation 2.25 is obtained.

$$ln(K_{eq}(T)) = -\frac{\Delta H^0_{adsorption}}{RT} + \frac{\Delta S^0_{adsorption}}{R} \tag{2.25}$$

Assuming the isosteric heat enthalpy to be the reverse of the excess enthalpy, i.e. the extra heat required to vaporize water from a solution due to solute activity, and setting $K_{eq} = a_w$, gives following van't Hoff equation [Mulet et al., 1999]:

$$ln(a_w) = \frac{\Delta H^0_{excess}}{RT} - \frac{\Delta S^0_{excess}}{R} \tag{2.26}$$

Where S^0_{excess} and $C^0_{p,excess}$ is the excess entropy and heat capacity. Though, this equation does not allow the enthalpy or entropy being dependent on temperature [Atkins and de Paula, 2002].

The following equations gives the temperature dependency of enthalpy and entropy

[Atkins and de Paula, 2002]:

$$\Delta H^0(T) = \Delta H^0(T_{ref}) + (T_{ref} - T)\,\Delta C_p^0$$
$$\Delta S^0(T) = \Delta S^0(T_{ref}) + \Delta C_p^0 ln\left(\frac{T}{T_{ref}}\right)$$

These expressions for the temperature dependence can be integrated in equation 2.26, to give an temperature dependent van't Hoff equation.
Defining a_w as the equilibrium constant in equation 2.26 gives an enthalpy related to the extra heat required to vaporize water [Mulet et al., 1999]. Therefore, relating this energy to the extra energy required to vaporize a solution, ΔH_{excess}, the water activity temperature dependency can be fitted with equation 2.27.

$$ln(K_{eq}) = \frac{\Delta H^0_{excess}(T_{ref}) + (T_{ref} - T)\,\Delta C_p^0}{RT} - \frac{\Delta S^0_{excess}(T_{ref}) + \Delta C^0_{p,excess} ln\left(\frac{T}{T_{ref}}\right)}{R} \tag{2.27}$$

The excess enthalpies, entropies and heat capacities might depend on concentration, as more water is bound at higher concentrations of solutes.

2.4 Temperature and Concentration Dependence of Sodium Chloride Solutions

The osmotic pressure of electrolyte solutions can be determined by the following equation [Clement et al., 2004]:

$$\Pi = -\frac{iRT}{\bar{V}_w} ln(1 - \gamma_{\pm} \cdot x_s) \tag{2.28}$$

Where i is the number of electrolytes in solution and $\gamma_{\pm}$ is the activity coefficient. This equation does not take account of the temperature dependence of the activity coefficient, $\gamma_{\pm}$. This has been determined by Cisternas and Galleguillos (1989). From this, a model of the temperature dependency of $\gamma_{\pm}$ can be carried out to determine the osmotic pressure of NaCl solutions at different concentrations and temperatures. This is described in further details in A on page 68. Equation 2.28 will be used to describe the osmotic pressure of NaCl solutions used in the experiments in this thesis.

3. Experimental

In order to examine if PPG 425 can be used as draw solution, it is necessary to examine how the osmotic pressure depends on concentration and temperature. Therefore, the osmotic pressure of different PPG 425 solutions at varying temperature will be determined by measuring the water activity. The water activities will be fitted to the van't Hoff equation 2.27 and BET isotherm 2.20 to express the temperature and concentration dependency of the osmotic pressure. This expression can be used in to model the flux in FO. To model the flux, the concentration and temperature dependency of the NaCl feed solutions has to be described. This will be done from 2.28 on the preceding page.
From the concentration and temperature dependency of the draw solution osmotic pressures, the optimal draw concentration and temperature can be determined, to give the highest possible flux.
The design of FO setup is inspired by McCutcheon et. al. (2006).
They use the thin CTA membrane from Hydrationtech, Inc. to obtain higher fluxes compared to RO membranes. To reduce strain on membrane, the crossflow was co-current 21.4 cm/s in a separation cell of two rectangular channels with the dimensions 7.7cm long, 2.6cm broad and 0.3 cm deep. A similar cell is designed in polysulfone.
To measure the flux of water, the draw container can be placed on a scale [McCutcheon et al., 2006]. The amount of water passing through the membrane is detected as the increase in weight of draw solution per time. Dividing this value with the membrane area gives the flux in $\frac{L}{m^2h}$. To equalize the increase in weight with the flux of water requires that the system connecting the draw container with the scale is filled with water only, and that no air bubbles or leaks interfere with the weight change. The scale also has to be precise to determine a change in weight from a low flux.
Since the osmotic pressure is temperature dependent, described in equation 2.5 on page 23, the temperature of the solutions will be controlled.
When a suitable PPG solution is found, various experiments will be conducted to find the optimum conditions for FO experiments with PPG 425 draw:

- Varying membrane thickness replacing the CTA membrane with a thicker membrane
- Varying membrane orientation
- Varying crossflow

The conditions with the highest measured flux are considered optimal. Using these, the flux is measured for different concentrations, i.e. different osmotic pressures, of draw and feed solutions. This is done to model the flux as a function of osmotic pressure with

equation 1.11 on page 17 or 1.13 on page 17. Since the flux will decrease with time, as the osmotic gradient decreases, it is only the start flux that will be used for modeling.
For the models, the membrane permeability will be measured. This is done by applying different hydraulic pressure of water to the membrane [McCutcheon et al., 2005]. The relationship between the flux and the pressure is the membrane permeability.
To predict the temperature dependence of the FO model, the van't Hoff plot or BET isotherm can predict the osmotic pressures temperature dependence. As the temperature also affects the characteristics of PPG solutions [Kirk, 1966, Weilby, 2008], the mass transfer coefficient of draw might also change with temperature. As stated in section 1.3 on page 13, k_D decreases with higher viscosity. Therefore the decrease in viscosity with temperature relates to the increase in mass transfer. The viscosity of PEG 2000 solutions decrease with higher temperatures, as a result of lower solubility of PEG [Hvidt, 2007]. The same tendency can be expected here, as PPG solubility decreases at increasing temperature. Therefore, the temperature dependence of a PPG solution will be studied to describe the temperature dependence of the concentration polarization.
To characterize the fouling of the FO membrane in this setup, an experiment is carried out for longer time, so a significant decrease in flux can be observed.
In order to ensure, that the membrane does not dissolve PPG molecules and contaminate the feed solution, a sample of feed from a filtration is analyzed with High Performance Liquid Chromatography (HPLC). Similar, the rejection of NaCl is measured in one filtration, using Atomic Absorption Spectrometry (AAS).
Figure 3.1 shows a phase diagram for PPG 400 [Malcolm and Rowlinson, 1957].

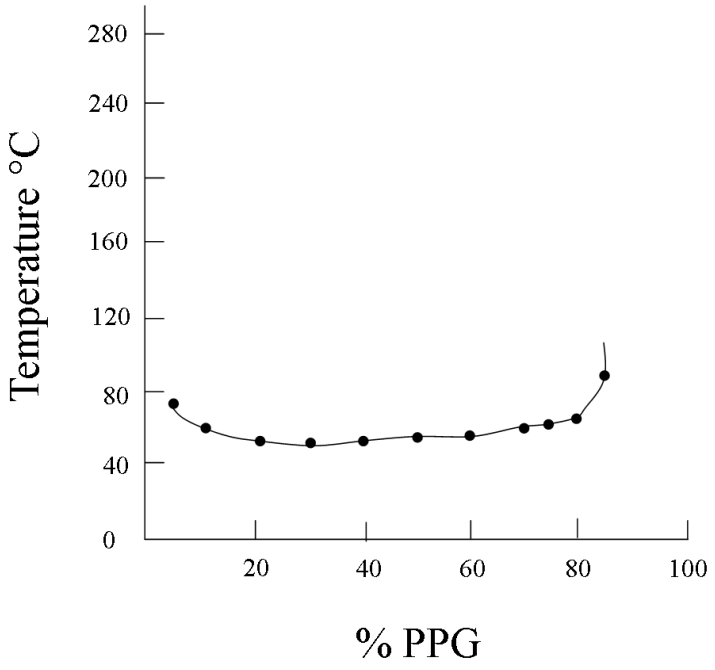

Figure 3.1: Phase diagram for water/PPG 400, inspired from Malcolm and Rowlinson (1957).

The phase diagram shows that between concentrations of 20 to 60 % PPG, the cloud point temperature is about 50 °C. As this sixe molecular weight shows separation, and because lower molecular weight PPG's are more hygroscopic than higher, PPG 425 solutions will be studied as draw solution. PPG 425 has an average molecular weight of 425 g/mol. As there are PPGs present with lower molecular weight, they might precipitate at higher temperatures [Kirk, 1966]. Therefore, it might be necessary to precipitate the PPG at even higher temperatures, than the cloud point temperatures. As PPG 425 is a liquid, PPG 425 solutions heated to over 50 °C gives a mixture of two insoluble liquids. The density of PPG 425 is 1.004 g/mL at 25 °C. Separation of such liquids can be catalyzed using a centrifuge at the given temperature [Clement et al., 2004].
The remaining PPG in the solutions can be detected with HPLC [Weilby, 2008]. Reversed-phase HPLC (RP-HPLC) can separate the different molar weights of PPG, and can be detected with an Refractive Index (RI) detector [Weilby, 2008]. The signal is proportional to the mass concentration of PPG. The expected lower concentration of PPG will be compared with molecular weights present before and after precipitation, measured with Mass Spectrometry.

3.1 Measuring water activity of solutions of Polypropylene Glycol 425

The water activity of PPG 425 solutions were measured on Aqualab 4TE (Devagon Devices, USA). The instrument can measure water activity with a precision of ±0.0030 between 15 and 50 °C. Sample cups were filled with 5 mL solutions with a 1-5 mL Finnpipette and placed in the instrument for measurement. The samples analyzed were 25, 30, 35, 40, 45 and 50 % PPG 425. The start temperature was 15 °C, and after measurement the temperature was increased with 5 °C until 50 °C is reached. This is except 50 % PPG 425, that was measured at temperatures between 15 °C and 50 °C with a 1 °C step. At temperatures below 20 °C, the instrument was placed in a cold room, in order to lower the demand of cooling the sample in the instrument. The sample mode was set to continuous, so the apparatus kept measuring until the water activity was estimated stable from at least three measurements.

3.2 Performing Forward Osmosis Experiments

Figure 3.2 on the facing page illustrates the experimental setup for forward osmosis experiments.

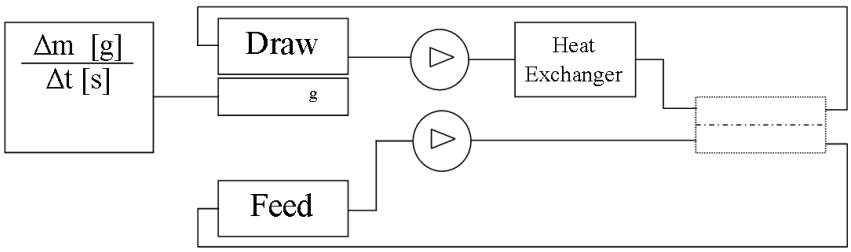

Figure 3.2: Experimental setup for forward osmosis. The draw solution container is placed on a scale to measure the flux over the membrane. From here, the draw solution is pumped to a heat exchanger, on to the separation cell and back to the container. The feed solution container is tempered with a heating mantle.

The draw solution container, a 100 mL graduated cylinder (±0.75mL, Silber Brand, Germany), was placed in a beaker filled with Polystyrene chips on a scale (±0.01g, OHAUS Adventurer ARC 120, China). From the scale, the solution was pumped through rubber tubings to the pump and on to the heat exchanger. The pump (Microgon Easyload, Masterflex, USA) had a dual pump head, so the tubing split in two parts, for double flow. The heat exchanger was a condenser, where the solution is pumped through the inner spiral, and water from a water bath tempered the solution from the volume between the mantle and the surrounding glass. From the heat exchanger the solution is pumped to the separation cell and back to the container.
The separation cells draw and feed chambers has dimensions 7.7cm x 2.6cm x 0.3cm (length x width x depth) and is cut in polysulfone. The cell is illustrated in figure 3.3 The scale is connected to a PC for logging data. The weight is logged every second.

Figure 3.3: FO cell with the two channels for draw and feed solutions.

The feed solution container was a round bottom flask with heating mantle. The feed solution was pumped through rubber tubings to the pump (Microgon Easyload, Masterflex, USA, with dual pump head), on to the separation cell and back to the container. The water bath (Lauda Ecoline RE104) pumps tempered water to the heat exchanger, then on to the feed container and back again.

Before every experiment, a new membrane (CTA, Hydrationtech, Inc., USA) is soaked in demineralized water for at least 30 minutes. 80 mL draw solution and 160 mL feed solution is measured and transferred to the containers with a 100 mL graduated cylinder (±0.75mL, Silber Brand, Germany). A thermometer is submerged in both the draw and feed solutions (AA precision, range -12-50 °C). The water bath was set to 13.5 °C and started to temper the heat exchanger and feed container, as the draw is circulated to the heat exchanger and back again. After at least 30 minutes the temperature is checked to be 15 °C ± 0.5 °C.
For analysis of osmotic pressure, 5 mL of both draw and feed is taken out with a 5 mL pipette (± 0.03 mL, Super Color, W. Germany). The samples water activity are measured at Aqualab at 15 °C.
Before analysis the pump is stopped, so the separation cell could be connected to the system. As logging of data is started, the pump is turned on. Bubbles accumulated in the separation cell are removed, and the time, where no bubbles are present in the system, is noted.
After each experiment, the system is drained for draw and feed solutions, and flushed with approximately 3 L of demineralized water.
The experiments performed are:

Varying Membrane Orientation

Experiments with 50 % PPG 425 draw and both 0 % NaCl and 0.5 % NaCl were conducted with the membrane support layer oriented against the draw solution, in addition to other experiments, where the support layer faces the feed solution.

Varying Membrane Type

Two experiments were performed with a so-called pouch membrane, 150 μm, instead of a CTA membrane (50 μm, Hydrationtech, Inc., USA). The solutions were 50 % PPG 425 solutions and 0.0, 0.5 and 1.5 % NaCl solutions.

Varying Crossflow

An experiment with 50 % PPG 425 draw and 0.4 % NaCl feed was conducted, adjusting the crossflow in the following order: 16.3, 20.0, 28.8 to 11.7 cm/s.

Varying Concentration of Feed Solutions

Experiments were performed with 50 % PPG 425 draw solutions and feed varied: 0.0 ((demineralized water)), 0.4, 0.5, 0.75, 1.0, 1.5, 2.0, 2.5 and 3.5 %. In the same manner,

experiments with 60 % PPG 425 and 0.0 (demineralized water) and 3.5 % NaCl were performed. The flux measured is modeled with least squares method in Excel.

Varying Concentration of Draw Solutions

These experiments were 0.4 % NaCl with varying solutions PPG 425: 0 (demineralized water), 40, 45, 50 and 60 %. The start flux was measured, and a single experiment using 50 % PPG 425 and 0.4 % NaCl run for 20 h.

3.2.1 Measuring Membrane Permeability

Two parts of CTA membrane (Hydrationtech, Inc., USA) were cut out to fit the RO separation cell for crossflow setup. The membrane areas were 0.026 m^2 and the crossflow set to 15000 L/h. The feed used was demineralized water. At different pressures, the permeate was collected in a bucket over 3 minutes and measured on a pre-tared scale (Mettler Toledo 3002-s). The crossflow pump was from Grundfos and the pressure pump was a Lewa LK1 (Germany).

3.2.2 Measuring Viscosity

Preparation

A 50 % PPG 425 was prepared the day before, put on a vibrating table at 3-4 ^{o}C for 24 hours. The viscosity was measured at temperatures from 10 ^{o}C to 30 ^{o}C at 5 ^{o}C intervals. About 35 mL sample was transferred to the sample container (CS double gap system, 40/50, Bohlin). Before measuring, the solution was tempered for 30 minutes. The samples were not filtrated.

Analysis

The viscosity was measured for 30 seconds at shear stresses increasing in the following order 0.05, 0.083, 0.139, 0.232, 0.387, 0.646, 1.077, 1.797, 2.997, 5.0 Pa and then decreases again in opposite order to 0.05. The viscosity was obtained fitting the collected data as a Newtonian fluid with Bohlin Software LUO 120 HRNF.

3.2.3 Analysis with Atomic Absorption Spectrometry

The samples analyzed are 1 % NaCl solution and 50 % PPG 425 solution after a 20 hour FO-filtration.

Preparation of Samples

Both the feed solution and the draw solution are filtered through a 45 μ micro filter to a vial weighed before and after the transfer (Mettler-Toledo AB 204-s)
A solution of 1000 mg/L Na is diluted to 100 mg/L Na. A standard addition sequence is performed for both solutions.

Feed solution The feed solution is diluted with 320 μL 2 M HNO_3. The feed solution is diluted 1000 times, first by transferring 1 ml feed solution to a plastic test tube along with 9 mL 0.1 M HNO_3, then by transferring 100 μL solution from the second plastic test tube to a third tube along with 9.9 mL 0.1 M HNO_3. 2.5 mL of the solution from the third plastic test tube is transferred into 4 tubes, numbered a-d. Tube a contained 2.5 mL of the 1000 times diluted feed, 0 μL 100 mg/L Na-solution and 7.5 mL 0.1 M HNO_3. Tube b contained 2.5 mL of the 1000 times diluted feed, 100 μL 100 mg/L Na-solution and 7.4 mL 0.1 M HNO_3. Tube c contained 2.5 mL of the 1000 times diluted feed, 200 μL 100 mg/L Na-solution and 7.3 mL 0.1 M HNO_3. Tube d contained 2.5 mL of the 1000 times diluted feed, 300 μL 100 mg/L Na-solution and 7.2 mL 0.1 M HNO_3.

Draw solution The draw solution is diluted with 370 μL 2 M HNO_3 and 2.5 mL of this is transferred into 4 tubes named e-h. Tube e contained 2.5 mL diluted draw, 0 μL 100 g/L Na-solution and 7.5 0.1 M HNO_3. Tube f contained 2.5 mL diluted draw, 50 μL 100 g/L Na-solution and 7.45 0.1 M HNO_3. Tube g contained 2.5 mL diluted draw, 100 μL 100 g/L Na-solution and 7.4 0.1 M HNO_3. Tube h contained 2.5 mL diluted draw, 150 μL 100 g/L Na-solution and 7.35 0.1 M HNO_3.

Analysis

The samples are then placed in an autosampler, Perkin Elmer AS-90 plus, and analyzed on the AAS, Perkin Elmer AAnalyst 100. Air-acetylen with an Na Intensitron Lamp (Perkin-Elmer, USA) is used.

3.3 Separation of Water from PPG 425 Solutions

Two methods are examined in order to find the one that separates most efficiently. These are centrifugation and precipitation. The separation was of 50 % PPG 425 at various temperatures. The water phases are then later analyzed for content of PPG. Also, a phase diagram is performed to determine where separation occurs.

3.3.1 Phase Diagram

Samples containing 5 %, 10%, 20%, 30%, 40%, 50%, 60%, 70%, 75% and 80% PPG 425 was submerged into a water bath. The temperature of this water bath was slowly raised from 25 ^{o}C - 76 ^{o}C one degree at the time with 5 minutes stagnation at each degree. The phase separation was determined by visual inspection. When a sample showed phase separation it was taken up.

3.3.2 Centrifugation

Preparation of Samples

The separation with centrifugation is analyzed at 55 and 60 ^{o}C. A 50 % PPG 425 is placed in a water bath with the same temperature as analyzed. Meanwhile, the Analytical Centrifuge (Lumisizer Dispersion Analyser, L.U.M. GmbH, Germany) is heated to this temperature. As the samples and the Lumisizer are tempered, the bottle containing the solution is shaked, and 500 μL sample is transferred to a centrifuge tube (Synthetic rectangular cell PC 2 mm, L.U.M. GmbH, Germany). The tube is then placed in the centrifuge.

Separation

The settings of the centrifuge are 500 rpm, measuring the transmission of light at different heights of the tube. 60 transmission profiles are recorded in intervals of 60 seconds for the total of one hour. After centrifugation, the water phases are transferred to eppendorf tubes.

3.3.3 Precipitation

5 mL of a 50 % PPG 425 solution is transferred to 10 ml plastic test tubes, and placed in a water bath (Grant, Y14). This is done for samples analyzed at 55, 60, 70 and 80 ^{o}C for either 1 or 2 hours. Though, the separation at 55 ^{o}C was only performed for 1 hour. After 1 or 2 hours, the water phase is extracted by a pipette and trasferred into a new test tube.

3.3.4 Analysis with Mass Spectrometry

PPG polymers are detected in water phases of 50 % PPG 425 after separation at 55 ^{o}C together with a sample of 50 % PPG 425.

Preparation of Samples

The samples analyzed are diluted 1:100 with 5 % formic acid.

Preparation of matrix

A 3 g/L solution of 2,5-dihydroxy benzoic acid (DHB) in TA2 is produced by dissolving 0.0045 g 2,5-dihydroxy benzoic acid in 1.49 mL TA2. TA2 is a mixture of acetonitril and trifluoroacetic acid in the proportion of 2:1 respectively. A filter consisting of C18-column material is transferred into a 2-20 μL Finn tip. The pipettetip filter is rinsed by 15 μL of 5 % formic acid. Then 10 μL of a sample is transherred through the filter, the C18-column material is retaining the PPG. The filter is rinsed again by 15 μL of 5 % formic acid. Finally 1 μL of DHB in TA2 is transferred to the filter, flushing the sample content from the C18 column material down to the Anchor Chip Plate. This filterproces is repeated with a new pippettefilter for each sample. 1 μL of reference, consisting of PEP mix and DHB in TA2 in equal volumens, are placed in two wells as references.

Analysis

The Anchor Chip Plate is placed in the MALDI-TOF mass spectrometer (Bruker Reflex III).

3.3.5 Analysis with High Performance Liquid Chromatography

The PPG content in the water phases from the separation experiments are measured. Furthermore, the presence of PPG in the feed solution of FO with 50 % PPG 425 and 0.4 % NaCl is analyzed.

Preparation of Samples

A standard sequence of PPG 425 dissolved in water, including an internal standard is performed. The concentrations consisted of: 0.1, 0.5, 1.0, 5.0, 10, 20, and 30 % PPG 425. The internal standard was present in all samples in concentration of 0.5 % 1-Propanol. Each sample of the water phase where added to a vial along with Propanol internal standard in 1:1 ratio of volumes. The compositions of eluents were 60 % Methanol (HPLC-Grade) and 40 % Milli-q-water.

Analysis

The standard sequence, a vial of only internal standard and the samples were placed in the autosampler (ASI-100, Dionex). The time of sample analysis of each sample was 25

minutes. The flow was 1 mL/min and the the injection volume 20 μL. The Column was a Jupiter 5U C18 300Å from Phenomenex, USA. The detector was an RI-101 (Shodex) and the pump P680 HPLC pump from Dionex.

4. Results

4.1 Osmotic Pressure of Polypropylene Glycol Solutions

The osmotic pressure of solutions of different concentration and temperature is presented in figure 4.1. The osmotic pressure is calculated from the measured water activities using equation 2.5 on page 23.

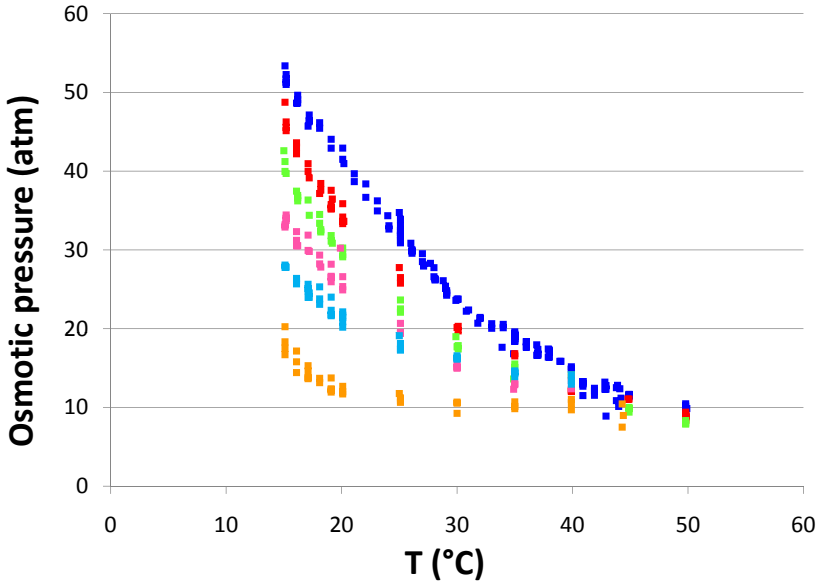

Figure 4.1: Osmotic pressure of different concentrations PPG 425 at varying temperature. ■ is 25%, ■ is 30%, ■ is 35%, ■ is 40%, ■ is 45% and ■ is 50%

The figure shows that the osmotic pressure decreases with higher temperature, as the solubility decreases. Also, the osmotic pressure increases with concentration, as stated in section 2.1 on page 22. At temperatures above 40 °C the osmotic pressures of the different concentrations are about 10-15 atm. At 50 °C the osmotic pressure is 8-10 atm, instead of 0 atm expected for a completely separated solution. As the measuring cup was taken out of the instrument at 50 °C it was observed, that separation has occurred. It is impossible to distinguish between the data, as they are all within the range of the apparatus uncertainties, ± 4 atm.

4.1.1 Ideality of Solutions

To study how the solutions deviate from ideality, $\frac{\Pi}{RTc}$ is plotted against the concentration, c 4.2 on the next page.

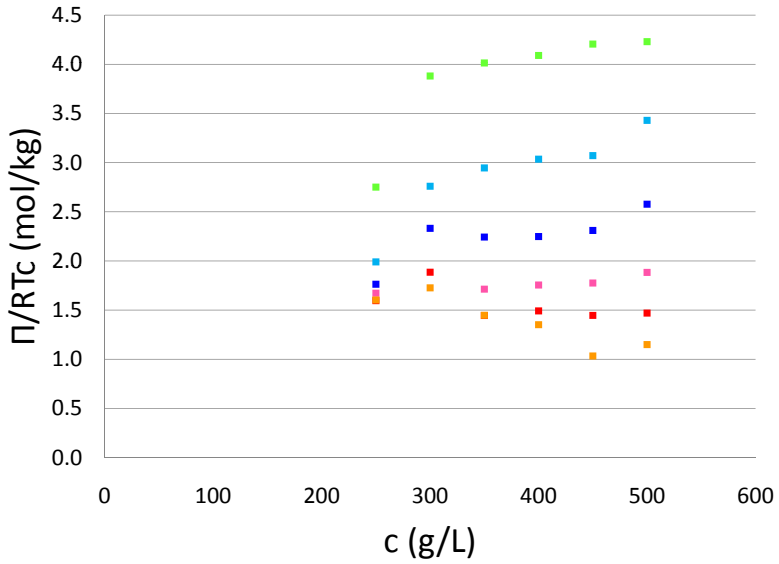

Figure 4.2: $\frac{\Pi}{RTc}$ plotted versus concentration for PPG solutions at different temperatures. ■ is 15 ^{o}C measured, – is 15 ^{o}C fitted. ■ is 20 ^{o}C, ■ is 25 ^{o}C, ■ is 30 ^{o}C, ■ is 35 ^{o}C and ■ is 40 ^{o}C.

The figure shows a tendency of increasing $\frac{\Pi}{RTc}$ with higher c. The data at 250 g/L (25 %) shows no linearity with the other data. From the linearity of the data from 300 to 500 g/L, 30 to 50 %, PPG 425, the parameters second virial coefficient, B', and molecular weight obtained from fitting the data to equation 2.17 on page 25 and presented in table 4.1.

Table 4.1: Fitted second virial coefficient, B, and molecular weights from plotting $\frac{\Pi}{RTc}$ versus c of PPG 425 solutions at different temperatures.

T ^{o}C	B'	g/mol
15	0.002	307
20	0.002	463
25	0.0011	534
30	-0.0011	762
35	-0.0016	458
40	-0.0031	390

The table show that B approaches zero as the temperature increases until 25-30 °C, where it becomes negative. The molecular weights determined from the linear intersection have a maximum in the same area. They are in the range of 307-762 g/mol, though all the solutions are of PPG 425.

4.1.2 Polypropylene Glycols Temperature and Concentration Dependence

The water activity concentration and temperature dependence is investigated by fitting the water activity to the linear BET isotherm, equation 2.20 on page 25. The data from

25 % PPG 425 was omitted from the fitting, as figure 4.2 on the previous page showed bad consistency with the data at 25 % compared to the rest of the data. In figure 4.3 the BET isotherms are presented.

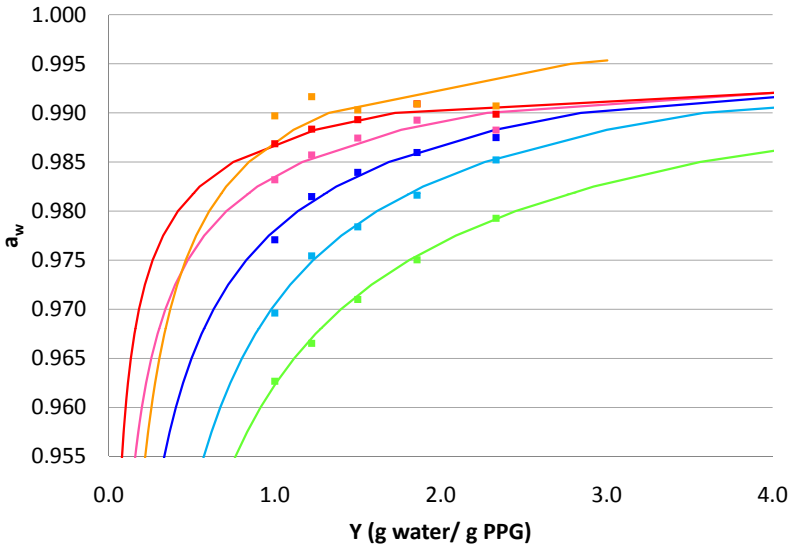

Figure 4.3: BET isotherms fitted to data for solutions of PPG 425 at different temperatures. ■ is 15 ^{o}C measured, ─ is 15 ^{o}C theoretical. ■ is 20 ^{o}C measured, ─ is 20 ^{o}C modeled. ■ is 25 ^{o}C measured, ─ is 25 ^{o}C modeled. ■ is 30 ^{o}C measured, ─ is 30 ^{o}C modeled. ■ is 35 ^{o}C measured, ─ is 35 ^{o}C modeled. ■ is 40 ^{o}C measured, ─ is 40 ^{o}C modeled.

The parameters from the fits are presented in table 4.2. From the constant j and equation 2.19 on page 25, ΔH^0_{excess} at different temperatures are calculated, and also presented in the table.

Table 4.2: BET parameters fitted from BET isotherms at different temperatures.

T ^{o}C g_{water}/g_{PPG}	Y_{mono}	j (J/mol)	ΔH^0_{excess}
15	0.073	0.042	-7852
20	0.04	0.085	-6124
25	0.038	0.031	-8576
30	0.056	0.007	-12360
35	-0.34	-0.0005	
40	0.015	0.097	-5774

Y_{mono} is positive at all temperatures except from 35 °C where it is negative. No clear correlation between temperature and excess enthalpy is observed. Therefore, the BET-isotherms can express the water activity as a function of concentration, but not temperature. Instead, the dependency of the water activity is described with van't Hoff plot, shown in the following figure 4.4:

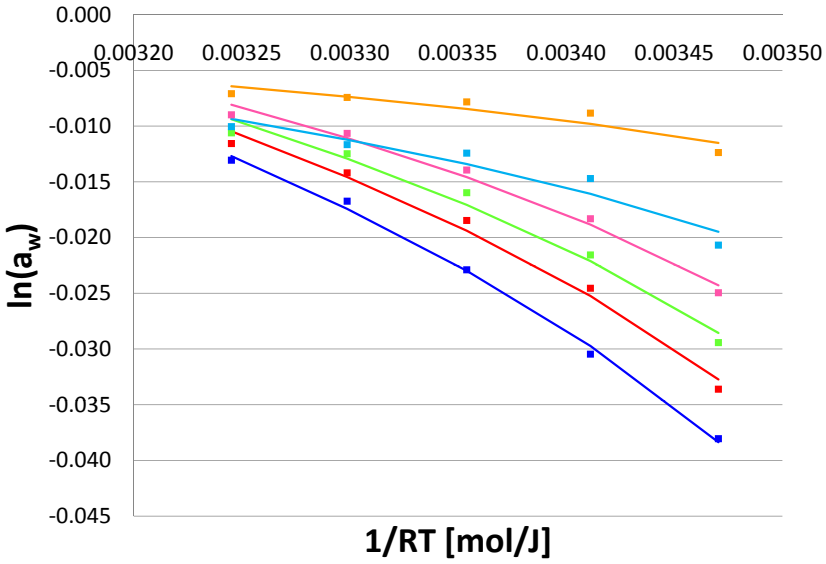

Figure 4.4: van't Hoff plot for different concentrations of PPG 425. ■ is 25% measured, ─ is 25 % modeled, ■ is 30% measured, ─ is 30 % modeled, ■ is 35% measured, ─ is 35 % modeled, ■ is 40% measured, ─ is 40 % modeled, ■ is 45% measured, ─ is 45 % modeled, ■ is 50% measured and ─ is 50 % modeled.

$\ln(a_w)$ decreases with higher $\frac{1}{RT}$, lower T, and lower concentrations at the 4 lowest temperatures plotted (15-30 ^{o}C). The fitted constants, excess enthalpy, entropy and heat capacity, for the van't Hoff plots at 25 °C given in figure 4.4 and presented in table 4.3.

Table 4.3: Excess enthalpies, entropies and heat capacities from van't Hoff plots at 25 °C

% PPG 425	$\Delta H^0_{excess}\,(25°C)$	$S^0_{excess}\,(25°C)$	$\Delta C^0_{p,excess}$
$J/(mol)$	$J/(mol \cdot K)$	$J/(mol)$	
50	113.0	-0.19	-0.31
45	97.0	-0.17	-0.27
40	83.4	-0.15	-0.23
35	70.6	-0.12	-0.19
30	43.5	-0.04	-0.12
25	21.5	-0.01	-0.06

The constants decrease with increasing temperature. They are fitted linearly as follows:

$$\Delta H^0_{excess}\,(25°C) = 3.6058 \cdot c_{\%mass} - 63.726, R^2 = 0.9802$$

$$S^0_{excess}\,(25°C) = -0.0076 \cdot c_{\%mass} + 0.1713, R^2 = 0.9417$$

$$\Delta C^0_{p,excess} = -0.0097 \cdot c_{\%mass} + 0.1682, R^2 = 0.9713$$

These are inserted into the van't Hoff equation, 2.27 on page 27, and combined with equation 2.5 on page 23, an expression of osmotic pressure of PPG 425 solutions as a

function of temperature and concentration is obtained.

$$ln\left(a_w\right) = -\frac{RT}{\bar{V}}\left(\frac{(3.6058\cdot c_{\%mass}-63.726)+\left(T_{ref}-T\right)(0.0076\cdot c_{\%mass}-0.1713)}{RT}\right)$$
$$-\frac{RT}{\bar{V}}\left(-\frac{-0.0076\cdot c_{\%mass}+0.1713+(-0.0097\cdot c_{\%mass}+0.1682)ln\left(\frac{T}{T_{ref}}\right)}{R}\right), R^2 = 0.9802 \qquad (4.1)$$

This is used to estimate the osmotic pressure of different solution concentrations at different temperatures in FO.

4.2 Settings for Forward Osmosis with Polypropylene Glycol Draw Solutions

To determine the membrane permeability of the CTA membrane, the permeate flow at different hydraulic pressures is measured. Dividing the flow with the membrane area and plotting this against the hydraulic pressure gives the correlation given in figure 4.5.

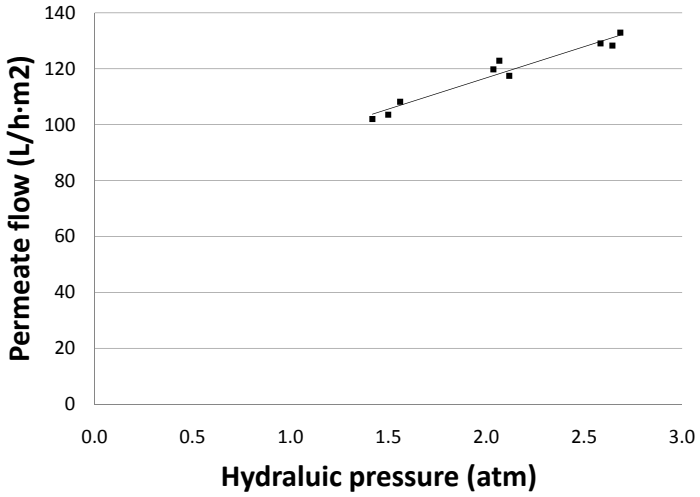

Figure 4.5: Permeate flow at different hydraulic pressures of water for a CTA membrane (Hydrationtech, Inc.

The slope of the line equals the membrane permeability, 9.76 $\frac{L}{h\cdot atm\cdot m^2}$. The intersection with the y-axis is 31.1 $\frac{L}{h\cdot m^2}$ and not 0 $\frac{L}{h\cdot m^2}$ as expected. The permeate flow was only measured at pressures lower than 3 bar, as higher pressures caused leakage from the separation cell.
In forward osmosis experiments flux was determined by logging the increase in weight of the draw solution for the first 10 minutes of the FO experiment, as illustrated in figure 4.6 on the facing page.

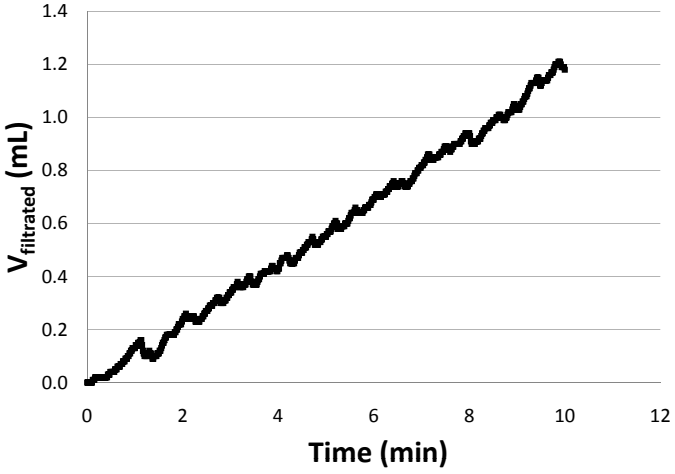

Figure 4.6: Increase of weight over time of 50 % PPG 425 against a water feed solution with a CTA membrane oriented with the support layer against the feed solution and a crossflow of 16.3 cm/s at 15 °C.

The curve is linear with some oscillations. During some of the experiments, a flow of air bobbles was observed. Though, there was no accumulation of air in the system.
The flux was determined by dividing the increase in weight with the membrane area of 0.002 m^2.
Using this strategy, fluxes from experiments, determining the optimum conditions for osmosis with PPG 425 draw, were measured and presented in table 4.4.

Table 4.4: Flux in $\frac{L}{h \cdot m^2}$ with 50 % PPG 425 draw at different NaCl concentrations, membranes and membrane orientations.

NaCl % (w/w)	CTA membrane dilutive ICP	CTA membrane concentrative ICP	Pouch membrane concentrative ICP
0	1.20	3.55	3.73
0.5	0.76	2.98	3.15
1.5	not performed	1.67	0.75

The experiments with dilutive ICP were performed with the membrane support layer facing the draw solution, as concentrative ICP experiments were with the support layer facing the feed solution. The table shows, that fluxes with dilutive ICP are lower than fluxes with concentrative ICP. Also, when no or low concentrations of NaCl feed is present, the Pouch membrane has fluxes in the same range as the CTA membranes fluxes. Though, at 3.5 % NaCl the flux is lower.
Varying the crossflow of both feed and draw gave the diagram presented in figure 4.7 on the following page from a 50 % PPG 425 solution and water feed.

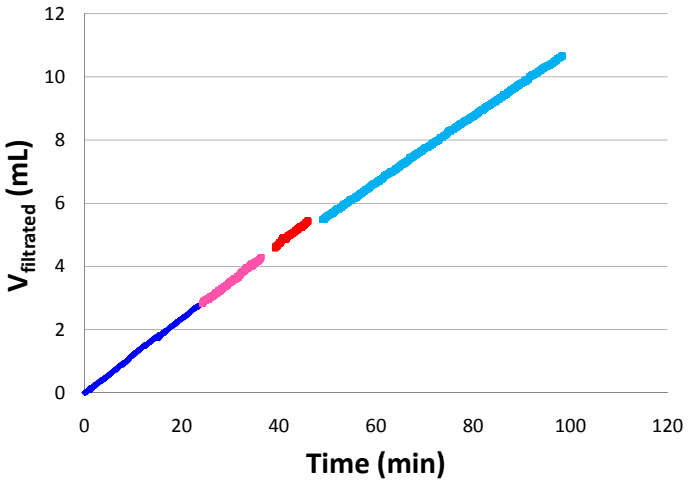

Figure 4.7: Increase in weight of 50 % PPG 425 against a water feed solution with a CTA membrane oriented with the support layer against the feed solution at 15 °C and variable crossflow. ■ is the flux at 11.7 cm/s, ■ is the flux at 16.3 cm/s, ■ is the flux at 20.0 cm/s, and ■ is the flux at 28.8 cm/s.

With crossflows 16.3, 20, 28.8 and 11.7 cm/s, the fluxes were 3.55, 3.58, 3.51 and 3.15 $\frac{L}{m^2 \cdot h}$ respectively.

4.3 Modeling Flux from Osmotic Pressure of Polypropylene Glycol and Sodium Chloride Solutions

Table 4.5 on the next page show the different FO experiments performed with varying concentrations of PPG 425 and NaCl. The calculated and measured osmotic pressures are also given together with the measured fluxes and the theoretical maximum flux. The osmotic pressures of PPG 425 solutions are calculated with equation 4.1 on page 42 and the NaCl osmotic pressures from equation 2.28 on page 27.

The measured fluxes are 2-40 times lower than theoretical fluxes without concentration polarization. The table also shows difference between measured and calculated osmotic pressure of up to 11 atm.
Figure 4.8 on the facing page show a series of FO experiments conducted with constant

Table 4.5: Overview of experiments with different concentrations draw and feed solutions. The measured and calculated osmotic pressures are given with the measured and theoretical fluxes and performance ratio. The osmotic pressure of the solutions from FO with 3.5 NaCl and 0 % PPG 425 was not measured.

PPG %	NaCl %	Π_D calc. (atm)	Π_F calc. (atm)	Π_D meas. (atm)	Π_F meas. (atm)	Jw meas. ($\frac{L}{h \cdot m^2}$)	Jw theoretical ($\frac{L}{h \cdot m^2}$)	Performance ratio %
50	0	52.8	0.0	56.9	0.0	3.59	68.45	5.2
50	0.4	52.8	2.6	51.5	5.3	3.25	65.14	5.0
50	0.5	52.8	3.2	54.5	7.0	3.19	64.25	5.0
50	0.75	52.8	4.9	54.9	8.1	3.06	62.04	4.9
50	1	52.8	6.6	58.4	8.7	1.84	59.83	3.1
50	1.5	52.8	10.1	52.1	11.5	1.50	55.42	2.7
50	2	52.8	13.5	55.0	14.6	1.23	51.00	2.4
50	2.5	52.8	16.9	49.7	17.4	1.11	46.58	2.4
50	3.5	52.8	23.7	41.2	26.1	0.83	37.75	2.2
0	0.4	0.0	2.6	0.0	3.9	-1.95	-3.32	58.7
40	0.4	38.9	2.6	39.2	6.4	3.73	47.12	7.9
45	0.4	45.9	2.6	46.0	4.6	2.23	56.13	4.0
50	0.4	52.7	2.6	51.5	5.3	3.25	65.14	5.0
60	0.4	66.7	2.6	67.3	8.7	4.29	83.15	5.2
60	3.5	66.7	23.7	66.8	23.5	1.24	55.77	2.2
0	3.5	0.0	23.7	-	-	-11.61	-30.70	37.8

concentration of feed solution at 0.4 % NaCl.

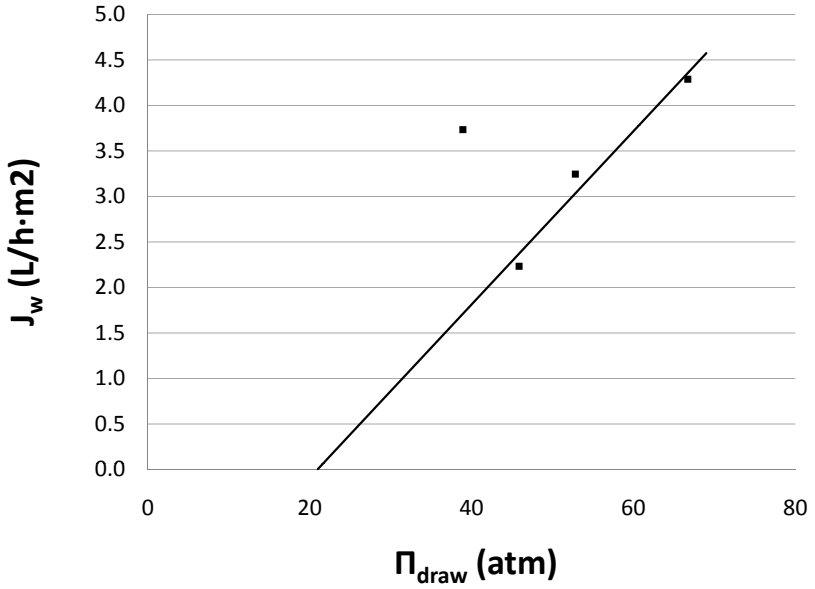

Figure 4.8: Fluxes at 0.4 % NaCl, 2.6 atm, and different osmotic pressures of PPG 425. ■ is data and ‾ represents linear fit of flux at 45-60 % PPG 425.

The linear regression of 60-45 % PPG 425 show decreasing flux with lower concentration of PPG 425, except from 40 % PPG 425, that causes a higher flux than both 45 and 50 % PPG 425. This is in spite, that the osmotic pressure, both measured and calculated, is lower than the osmotic pressures of 45, 50 and 60 ^{o}C PPG 425.
In figure 4.9 fluxes from FO with varying feed concentrations and 50 % PPG 425 solutions are presented.

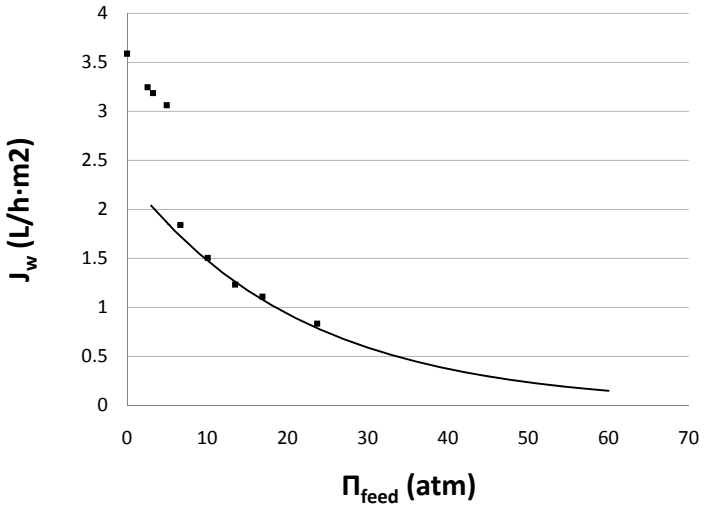

Figure 4.9: Flux at 50 % PPG 425, 52.8 atm, and different osmotic pressures of PPG 425. ■ is data and ‒ is an exponential fit of the flux at 1-3.5 % NaCl

The exponential regression of the flux from 3.5 to 1 % NaCl shows increasing flux with decreasing osmotic pressure of feed. Though, at 0.75 % NaCl the flux increases more than expected, and overall, there is not an exponential behavior. The exponential increase in flux with lower feed concentration, as expected from equation 1.13 on page 17 is not observed. Therefore, it was not possible to fit all the data in one model presented in table 4.5 on the previous page. Instead, the data are fitted in two series; one for NaCl concentrations 0-0.75 % NaCl, Model A, and one for NaCl concentration 1-3.5 % NaCl, Model B. Also, flux obtained from FO with draw solutions of 40 and 0 % PPG are omitted from the fitting of the models. The data are fitted to equation 1.13 on page 17 with the least squares method in the Solver function in Microsoft Office Excel. This is done, determining the lowest sum of squared errors between the modeled and experimental data. The error is minimized, changing the parameters A, k_D and $k_{CP,F}$.
Model A, valid for NaCl 0-0.75 % NaCl, 0-4.9 atm, is presented in figure 4.10 on the next page with both the model from measured osmotic pressures and the model fitted from calculated osmotic pressures. For draw concentrations fixed at 50 % PPG, the flux is plotted against the osmotic pressures of NaCl, and at feed concentrations fixed at 0.4 % NaCl, the flux is plotted against the PPG 425 osmotic pressure.

For Model A, the fitted parameters are: A=0.0713 $\frac{L}{atm \cdot h \cdot m^2}$, k_D= 34.12 $\frac{L}{h \cdot m^2}$ and $k_{CP,F}$= 57.02 $\frac{L}{h \cdot m^2}$. For the model fitted to data from calculated and experimental osmotic pres-

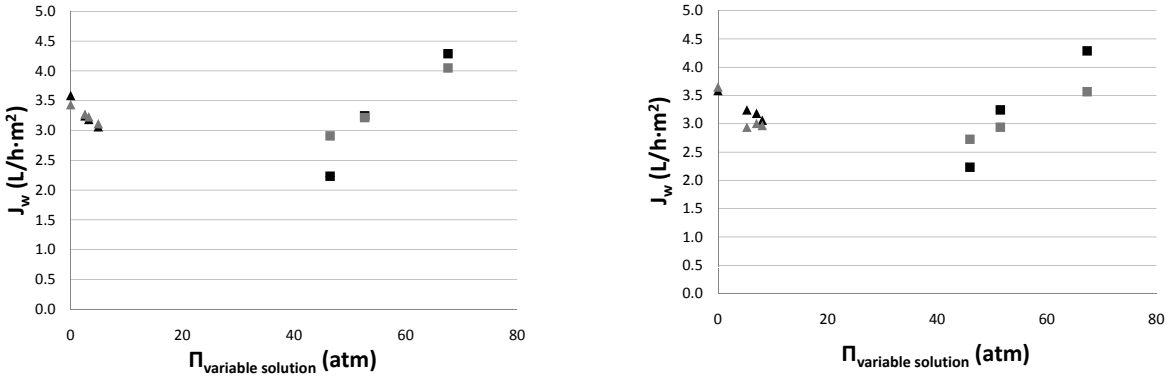

Figure 4.10: Flux at different osmotic pressures of feed and draw solutions. The model is based on feed concentrations 0-0.75 %, i.e. osmotic pressure between 0 and 4.9 atm. The data in the left diagram are based on calculated osmotic pressures, and the data in the right diagram are from experimental osmotic pressures. ■ is experimental flux when varying draw, ■ is modeled flux when varying draw, ▲ is experimental flux when varying feed and ▲ is modeled flux when varying feed.

sures, R^2 equals 0.88 and 0.56 respectively.

In the same manner Model B, using NaCl concentrations 1-3.5 % NaCl, 6.7-23.7 atm, is fitted to flux with both calculated and osmotic pressures. In figure 4.11 measured and fitted data are presented for NaCl concentrations 1-3.5 % NaCl.

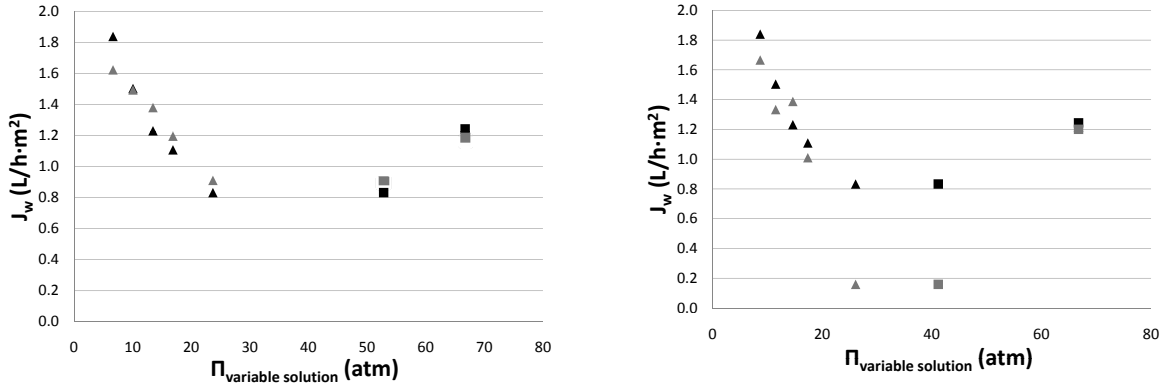

Figure 4.11: Flux at different osmotic pressures of feed and draw solutions. The model is based on feed concentrations 1-3.5 %, i.e. osmotic pressure between 6.7 and 23.7 atm. The data in the left diagram are based on calculated osmotic pressures, and the data in the right diagram are from experimental osmotic pressures. ■ is experimental flux when varying draw, ■ is modeled flux when varying draw, ▲ is experimental flux when varying feed and ▲ is modeled flux when varying feed.

The fitted parameters for Model B are: A=0.0558 $\frac{L}{atm \cdot h \cdot m^2}$, k_D= 7.20 $\frac{L}{h \cdot m^2}$ and $k_{CP,F}$= 3.21 $\frac{L}{h \cdot m^2}$. R^2 values are 0.88 and 0.07 for the model fitted to data based on calculated and experimental osmotic pressure, respectively.

The obtained models are used to describe the fouling of the membrane in two experiments. This is done for the FO filtrations of 3.5 % NaCl with 60 % PPG 425 and 0.4 % NaCl with 50 % PPG 425. Figure 4.12 on the next page shows the volume of water drawn from

feed solution over time from these experiments and calculated from Model A and Model B, taking regard to dilution and concentration of the draw and feed solution, respectively.

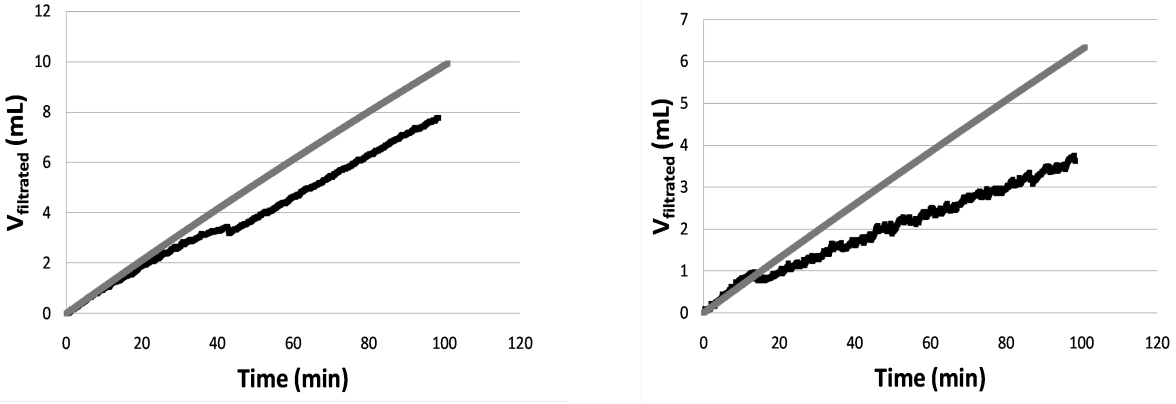

Figure 4.12: The volume of water filtrated of both measured, ■, and modeled, ■, data. At left data from 50 % PPG 425 - 0.4 % NaCl FO and right from 60 % PPG 425 - 3.5 % NaCl FO.

The start flux of the experimental data and the modeled data are similar, but after about 15 minutes, the measured flux decrease, giving a slower transfer of water than modeled. The increase in weight, of the solutions, decrease with time. This decrease in flux, is faster for the experimental data than the modeled data. Figure 4.12 also shows that the difference in flux is higher in the experiment 60 % PPG draw - 3.5 % NaCl feed. After 20 h the flux has decreased from 3.25 $\frac{L}{m^2 \cdot h}$ to 1.85 $\frac{L}{m^2 \cdot h}$ in the 50 % PPG 425 draw and 0.4 % NaCl FO experiment. The draw solution is diluted to a 23 % solution and the feed solution is concentrated to 0.86 %. From the solutions after 20 h, the rejection of salt is determined with AAS.

4.3.1 Rejection of salt

Figure 4.13 on the next page shows the standard addition of sodium ions to feed and draw solutions from 50 % PPG 425 - 0.4 % NaCl FO, after 20 h filtration.

The intersection with the x-axis of the linear regressions is the amount of sodium ions present in the diluted samples, and can be calculated from the linear regression fitted to the data.
The diluted PPG solution, diluted four times, shows the following linear relationship between intensity and added sodium ions:

$$Intensity = 0.3589 \cdot c_{Na^+added} + 0.833, R^2 = 0.994$$

From this the intersection with the x-axis is determined to -2.32 mg/L, i.e. there are 9.3 mg/L sodium ions, corresponding to 0.0024 % NaCl.

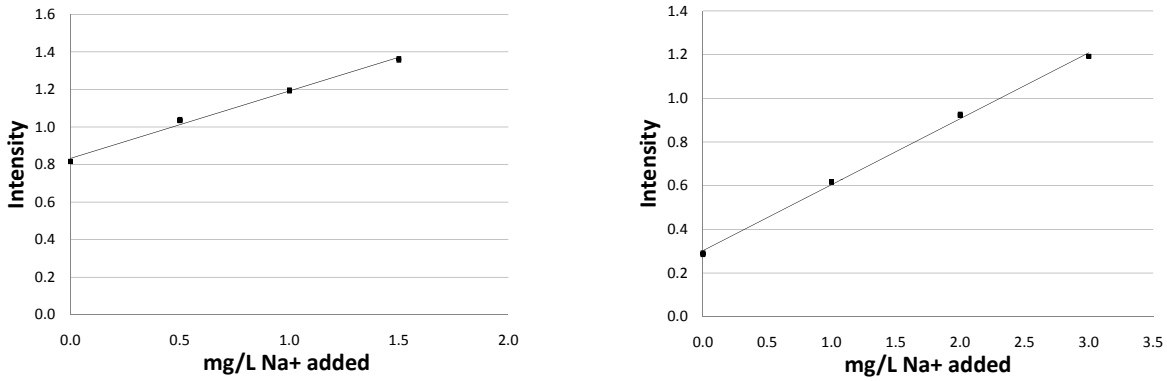

Figure 4.13: The diagrams show the intensity of samples with different amounts of sodium ions added, obtained from AAS analysis. In the left diagram, the sample is filtrated 50 % PPG 425, and the right is filtrated 0.4 % NaCl.

The feed solution, diluted 4000 times, show the following relationship:

$$Intensity = 0.302 \cdot c_{Na^+added} + 0.3026, R^2 = 0.9979$$

Similarly, the concentration of NaCl is determined to be 1.02 % From these data and equation 1.2 on page 12, $r_{rejection}$ is determined:

$$r_{rejection} = 1 - \frac{0.0024\%}{1.02\%} = 0.998$$

4.3.2 Viscosity of PPG 425

The temperature dependence of the viscosity of a 50 % PPG 425 solution was measured. The viscosities presented in figure 4.14 were calculated fitting the data as a newtonian fluid. At all temperatures the data fitted with an R^2 above 0.99.

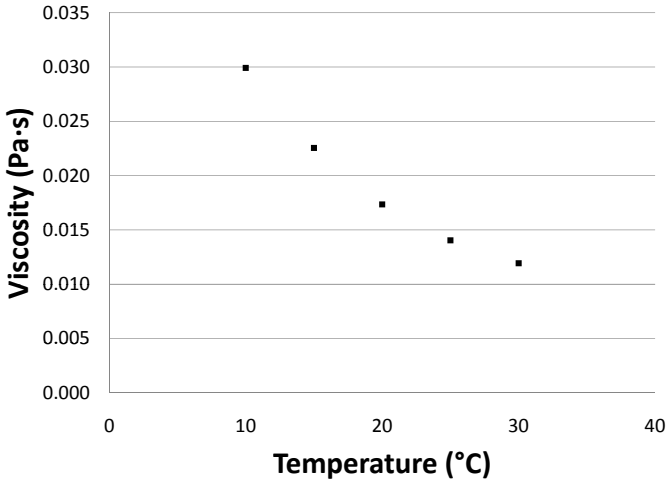

Figure 4.14: The viscosity of 50 % PPG 425 at different temperature.

The viscosity decreases with increasing temperature, as the solubility of the PPG decreases. Therefore, k_D might increase when the temperature is lowered.

4.4 Separation of Polypropylene Glycol Solutions

In figure 4.15, the phase diagram for PPG 425 is presented.

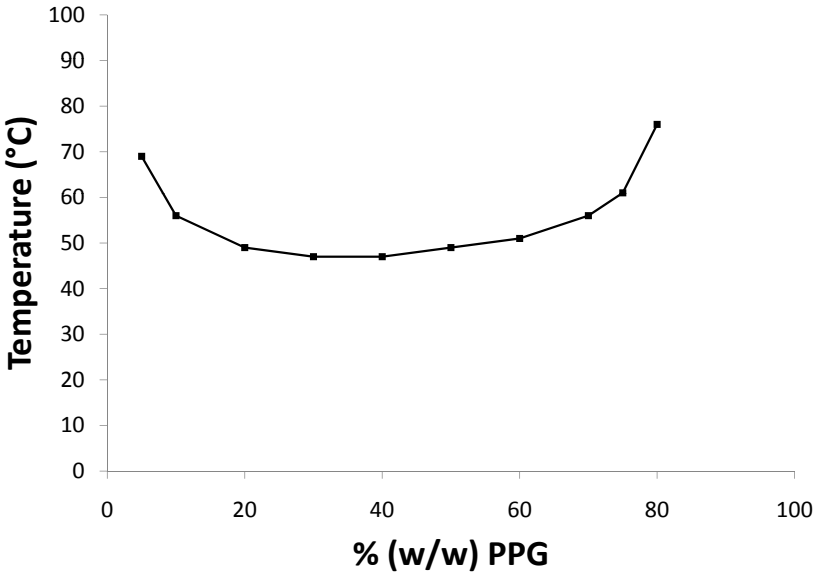

Figure 4.15: Phase diagram for PPG 425.

The separation was observed, as the solutions became turbid. In agreement with the phase diagram presented in figure 3.1 on page 29, the cloud point temperature for concentrations 20 to 60 % PPG, is approximately 50 °C, and it increases at higher and lower concentrations. The cloud points are observed, as the solutions turn white and precipitate.
In figure 4.16 on the facing page, the transmission profiles through the test tube during centrifugation of 50 % PPG 425 at 55 ^{o}C is given, after 4, 20 and 28 minutes.

The transmission after 4 minutes show low transmission, i.e. the light is blocked. This is in accordance, with the solutions being white in the start of the separation, as observed when performing the phase diagram. After 20 minutes, the upper part of the solution turns almost transparent, while the part, that is in the lower 10 mm of the tube still has a transparency of about 50 %. After 28 minutes, both the upper and lower part of the tube has a transparency from 80 to 100 % with a separation between the upper and lower phase at about 10 mm. The same tendency was observed at centrifugation at 60 ^{o}C

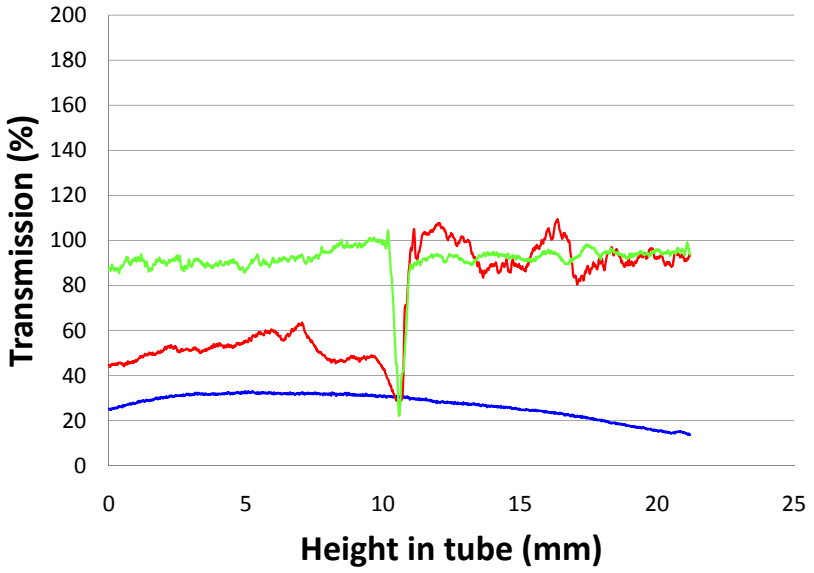

Figure 4.16: Transmission profiles at 4, 20 and 28 minutes in test tube with 50 % PPG 425 at 55 ^{o}C during centrifugation at 500 rpm. – is after 4 minutes, – is after 20 minutes, and – is transmission after 24 minutes.

4.4.1 Characterization of Separation with Mass Spectrometry

A 50 % PPG 425 solution before separation was analyzed with Mass Spectrometry, shown in figure 4.17 on the next page.

The masses detected are similar to masses of different sizes polymers minus the mass of the hydroxy end groups. This was also observed on Mass spectra of water phases from 50 % PPG 425 solutions separated at 55 °C with precipitation and centrifugation for one hour, presented in figure 4.18 on the following page

The intensities of PPGs detected in the 50 % PPG 425 solution shows a gaussian distribution of PPGs with the highest intensity at PPG 621 (i.e. PPG 655). Though, PPG 273 and 331 are not a part of this distribution. However, the water phases from separated solutions show gaussian distributions with mean molecular weights of PPG at 505 and 447 (539 and 481). Assuming, that the intensities can be related to molar concentrations, gives an weight average molecular weight of 494 g/mol and 512 g/mol of PPGs present in water phases of centrifuged and precipitated 50 % PPG 425 solutions. For the 50 % PPG 425 solution analyzed, the average molecular weight is 593 g/mol.

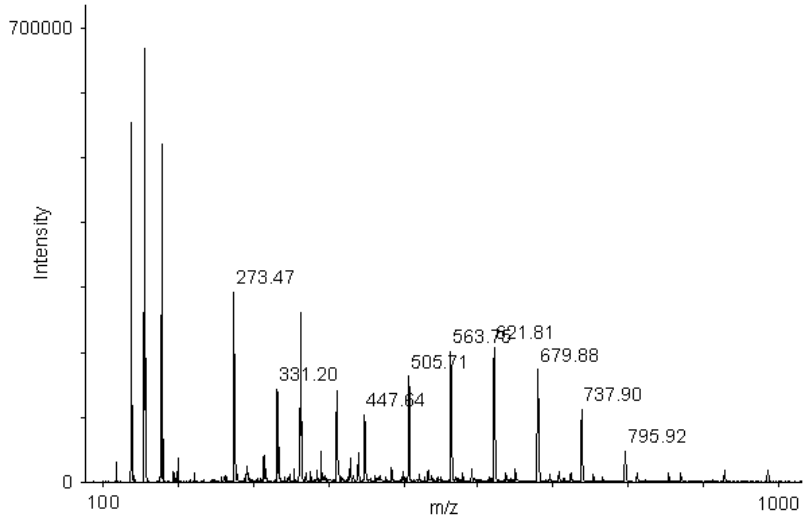

Figure 4.17: Mass Spectrum of 50 % PPG 425 before separation. The numbers given at the peaks are molecular weights.

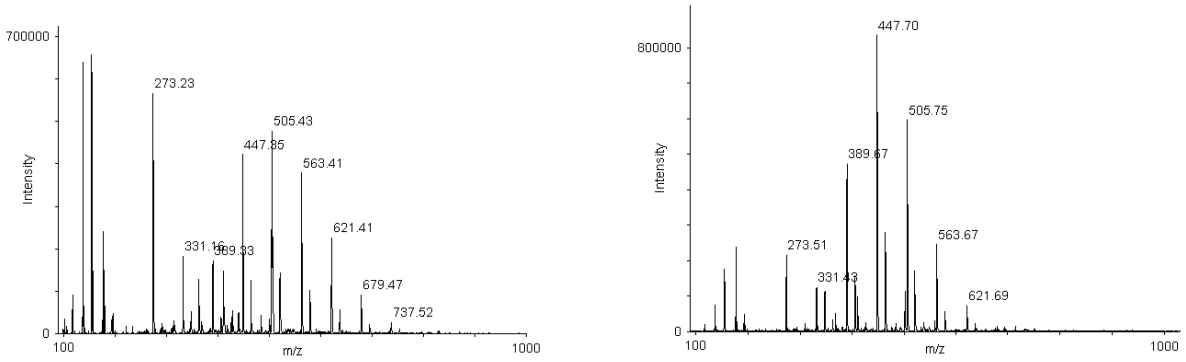

Figure 4.18: Mass Spectra of, at left, water phase from precipitated 50 % PPG 425 and at right water phase from centrifugated 50 % PPG 425. The numbers given at the peaks are molecular weights.

4.4.2 Characterization of Separation with High Performance Liquid Chromatography

The following figure shows the HPLC-RI spectrum obtained from a 1 % propanol solution.

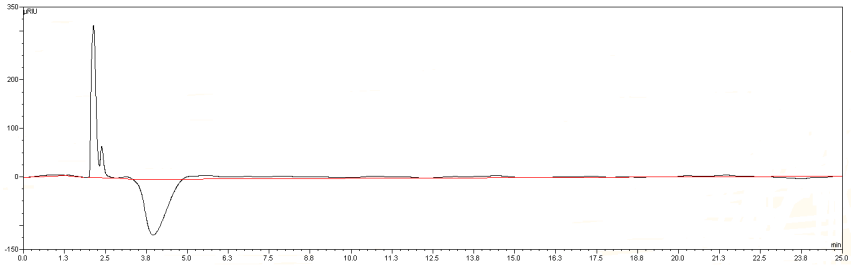

Figure 4.19: HPLC-RI spectrum of 1 % propanol in water.

At all spectra there is a peak after 2.13 minutes, t_m, i.e. the peak is from eluent and unretained solute. The spectrum shows a peak after 2.38 minutes, i.e. the corrected retention time of propanol internal standard, is $t_{r,propanol}$ =2.38-2.13 minutes $\approx$ 0.25 minutes. After about 4 minutes a drop in signal was observed. This was present in all spectra of all samples, and interfered with some of the signals from PPG, as presented in figure 4.20. Changing the mobile phase composition did not affect the peak.

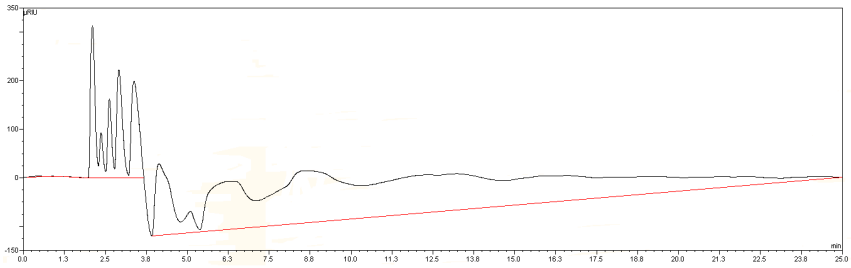

Figure 4.20: HPLC-RI spectrum of 10 % PPG with 1 % propanol internal standard.

The figure shows, that only the two first PPG peaks at $t_{r,propanol}$ approximately 0.6 and 0.9 minutes (2.7 and 3.1 minutes in figure 4.20) could be used. Though, no total concentration of PPG could be determined. Instead, the decline in concentration of the PPG from the first two peaks could be described using the following standard curve:

The standard curves are obtained, plotting the area of PPG peaks divided by the area of propanol peak, with the area of the propanol.
From the fitted standard curves the decrease in percent of mass concentration of the PPG from peak 1 and 2, is given in table 4.6 on the next page.

The decrease in concentration of PPG from peak 1 varied from 36.1 to 61.1 % for the different separation strategies. The decrease of PPG from peak 2 varied from 43 to 74.2 %.

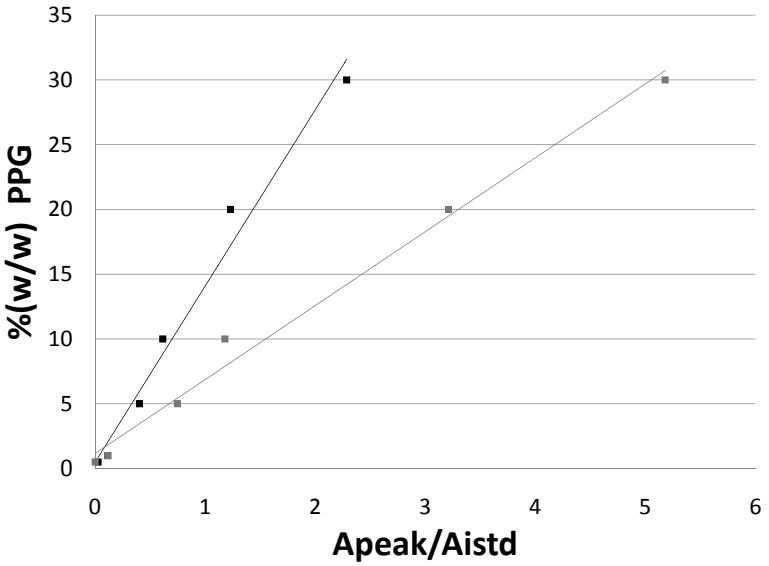

Figure 4.21: Standard curve for total PPG concentration dependence of $A_{peak}/A_{peak,istd.}$ for PPG peak 1 and 2. ■ is from peak 1 and ■ is from peak 2.

Table 4.6: Decrease in concentration of PPG from peak 1 and 2 in water phase after separation with precipitation and centrifugation with varying temperature and time.

Method	Temperature	Duration	Decrease in concentration peak 1 (%)	Decrease in concentration peak 2 (%)
Centrifuged	55 °C		36.1	43.8
-||-	60 °C		46.1	55.2
Precipitated	55 °C	1 h	44.7	53.5
-||-	60 °C	1 h	49.5	61.1
-||-	60 °C	2 h	25.0	43.0
-||-	70 °C	1 h	56.5	68.4
-||-	70 °C	2 h	56.1	68.0
-||-	80 °C	1 h	59.7	73.1
-||-	80 °C	2 h	61.2	74.2

The decrease in PPG concentration was lower for centrifuged samples than precipitated samples. According to the table, more time for precipitation does not induce further decrease in concentration. Though, at higher temperatures, the separation of water from PPG solutions is more effective. Also, it is seen that decrease in concentration of peak 2 is higher than peak 1.

5. Discussion

Osmotic Pressure of Polypropylene Glycol Solutions The first objective of this thesis is to describe how the osmotic pressure of PPG 425 solutions relates to the temperature and concentration of PPG solutions.

The measured water activities in figure 4.1 on page 38 show high osmotic pressures of the PPG 425 solutions at lower temperatures, where the solubility is higher. The ideality of the solutions is described with the second virial coefficient, B, given in table 4.2 on page 39. It is positive at temperatures below 25 ^{o}C. At temperatures over 30 ^{o}C, B indicates osmotic pressures lower than of an ideal solutions. This might be caused by the lower solubility of PPG at higher temperatures. A negative B', i.e. the osmotic pressure is lower than for ideal solutions, means that some of the polymers are not in solution any longer. Though, no precipitation of polymers was observed at temperatures 25-30 ^{o}C. Therefore the negative B' is more likely a result of uncertainties of measuring at high temperatures where the water activities are close to 1, and the difference small.

The average molecular weight determined is in a range from 307 to 762 g/mol, in accordance with the average molecular weight of 425 g/mol given by the manufacturer. As it is determined from the intersection with the secondary axis, it will be affected by an uncertainty of the slope. Though, the mass spectrum for a 50 % PPG 425 solution presented in figure 4.17 on page 52 shows the presence of PPG 308 - PPG 830. Presumed, that the intensity is proportional to the molar concentration, the average molecular weight is 593 g/mol which is higher than 425 g/mol. If this is the case, the osmotic pressure measured is not the osmotic pressure of a PPG 425 solution, but a PPG 593 solution, and thus lower. The gaussian distribution also shows a higher amount of higher molecular weight PPG present, with PPG 308 and 366 diverging from this distribution. Though, there are some uncertainties, setting the signal proportional to the molar concentration, as different length polymers are ionized different in MS. Furthermore, the phase diagram in figure 4.15 on page 50 is similar to the phase diagram for PPG 400 presented in the literature, figure 3.1 on page 29, indicating, that the solution is consistent with a PPG 425 solution.

The BET isotherms was fitted to the water activities at different concentrations, presented in figure 4.3 on page 40. At 40 ^{o}C the data does not fit the model, as the water activities at this level are in the range of the uncertainties of the instrument, $\pm$ 0.0030. The parameters, j and Y_{mono}, does not prove any temperature dependence. This might be a result of the water activity fitting only in the interval of approximately 0.95-1, and not in the full range, 0-1. As the parameters does not show temperature dependency, the BET isotherm was not used for further analysis.

The plot of $ln(a_w)$ versus $\frac{1}{RT}$ presented in figure 4.4 on page 41 shows bending curves,

indicating that the excess enthalpy is temperature dependent. Again, the data differ from theory at temperatures above 25 ^{o}C, as ln(a_w) for 35 % PPG 425 here is higher than 30 % PPG 425, i.e. the osmotic pressure of the higher concentration is lower than the lower concentration PPG. Because the water activities measured at and above 40 ^{o}C were too imprecise, only the data below 40 ^{o}C was fitted to the extended van't Hoff equation, 2.27 on page 27. The fits are consistent with the data of different concentration. The parameters from the fit show a linear correlation to the concentration. Fitting the temperature dependent van't Hoff plot with experimental data gives fits that corresponds to the experimental data. Because ΔH^0_{excess} for the different concentrations is possitive, the solutions demand more heat to vaporize water than fresh water. The enthalpy shows a linear relationship with concentration. Therefore, the higher concentration of PPG, the more heat is needed to vaporize water, in accordance with the osmotic pressures dependence on concentration. As $\Delta S^0_{p,excess}$ and $\Delta C^0_{p,excess}$ also can be described by the concentration of PPG, equation 4.1 on page 42 is used to express the osmotic pressure of water at different temperature and concentration. Though, it is only valid in the range of temperature from 15 to 35 ^{o}C and 25 to 50 % PPG 425.

Flux Dependence of Experimental Settings From this expression, and from the measured data, the optimum conditions for FO, in order to maintain the highest flux is stated to be at low temperatures and high concentrations. Therefore, solutions of 50 % PPG 425 was used as draw solutions at 15 ^{o}C.

In table 4.4 on page 43 the flux at different membrane thickness is presented. At low concentrations of NaCl, the flux is almost the same using a thin CTA membrane and a thicker pouch membrane. Then, at 1.5 % NaCl, the flux decreased to be less than half of the flux, using the CTA membrane. This is caused by the thicker membrane as described in section 1.3 on page 13.

The flux measured at different membrane orientations, presented in table 4.4 on page 43, showed that concentrative ICP gives a higher flux of water in the case of PPG draw and NaCl feed solutions. This is because, the ICP depends on how fast that the solutes counter-diffuse the concentration polarization. As PPG polymers are larger molecules compared to sodium and chloride ions, they are slower. Therefore, the concentration polarization is highest as the membrane support layer faces the PPG solution instead of the NaCl solution. Though, if a feed solution with high fouling potential is used, it might be necessary to face the support layer against the PPG draw solution. This will prevent high fouling but also cause higher CP from PPG.

The influence of concentration polarization by PPG is also observed in experiments with demineralized water instead of PPG, presented in table 4.5 on page 45. As the NaCl has higher osmotic pressure than the water, the flux is turned, and the ICP is dilutive.

The performance ratio in the experiments without PPG is about 38-59 %. This is approximately 10 times higher than in experiments with PPG draw. As the ICP is dilutive and therby having another solute resistance to diffusion, these fluxes were not used for modeling.
Even though the ECP by PPG is high compared to the CP by NaCl, the flux does not seem to increase with higher crossflow, as given from figure 4.7 on page 44. Two different explanations can reveal the causes: Either, varying crossflow cannot decrease the boundary layer thickness further, or much higher crossflow is necessary to observe an impact on the layer thickness. As almost no impact on flux from changing the crossflow from 11.7 to 28.8 cm/s is observed, it is believed, that the boundary layer thickness cannot be reduced further by increasing crossflow. The small change in flux with crossflow observed could as well be uncertainties or due to dilution and concentration of draw and feed solution. Therefore, it is concluded, that varying the crossflow did not have impact on flux.

Flux Modeling from Osmotic Pressures From table 4.5 on page 45 it is given, that at experiments using 45 to 60 % PPG 425 draw, the performance ratios are in the range 2.2-5.2 %. Though, in one experiment using 40 % PPG 425 draw, the performance ratio is 7.9 %. The flux using 40 % PPG 425 draw - 0.4 % NaCl is even higher than the flux obtained with 50 % PPG 425 draw solution, even though the osmotic pressure is 20 % lower. This indicates, that the ECP of 40 % PPG 425 is lower than 50 % PPG 425, i.e. k_D is concentration dependent. This can eventually be a cause of lower viscosity of 40 % PPG 425 than 50 % PPG 425. This can be revealed with more experiments using 40 % PPG 425 draw and comparing the viscosity of 40 % with the viscosity of 50 % PPG 425. Besides from 40 % PPG 425, increasing draw osmotic pressures gives higher fluxes as given from figure 4.8 on page 45. The linear regression from these data given in figure 4.8 on page 45 show a flux of 0 $\frac{L}{h \cdot m^2}$ at 20 atm instead of 0 atm. This may be caused by CP and uncertainties from a three point regression. In experiments with 50 % PPG 425, decreasing osmotic pressure of NaCl feed shows a decrease in flux. The flux approaches 0 $\frac{L}{h \cdot m^2}$ over 60 atm, even though the osmotic pressure of the draw solutions are 52.8 atm. This may be a consequence of bad modeling caused by few data points, rather than CP, as CP should lower the intersection with the primary axis. Though, the exponential increase caused by ICP does not occur, as the flux increase significantly and unexpected at osmotic pressures of feed solutions below 0.75 % NaCl. This shows, that a lower than expected CP by NaCl is present at concentrations at and below 0.75 %, i.e. 4.9 atm. This suggests, that there is a limit at 0.75 % NaCl, and at concentrations above this, the CP by NaCl gets significant. Another point of view is, that the data from 3.5 to 0.75 % NaCl follow an exponential increase with lower osmotic pressure. This increase levels of at feed osmotic pressures below 0.75 % NaCl, resulting in a lower than expected flux. An explanation

for this phenomenon would be, that the increasing flux gives a faster dilution of the draw solution, and thus higher ECP. This should, however, be described by equation 1.13 on page 17. The performance ratios for the flux obtained below 0.75 % NaCl feed solution are higher than those from above this concentration. This rejects the theory of the lowest concentrations giving the highest overall CP. Because it was not possible to fit the flux equation for the entire set of data, the dataset was split in two, and fitted separate.
The models obtained has water permeabilities of A=0.0713 $\frac{L}{atm \cdot h \cdot m^2}$ and A=0.0558 $\frac{L}{atm \cdot h \cdot m^2}$ for Model A and Model B respectively. These are lower than the measured 9.76 $\frac{L}{h \cdot atm \cdot m^2}$ and the value given in the literature, A=1.12 $\frac{L}{h \cdot m^2}$. The measured water permeability could be higher than the actual as a consequence of the membrane being damaged. This is consistent with the intersection at the secondary axis, telling that at 0 atm pressure, the membrane transports 31.1 $\frac{L}{h \cdot m^2}$ water. The leakage intensified at pressures above 3 atm, where the RO separation cell cell started to leak. This can be caused by inaccurate cutting of membrane. The difference between A modeled and A from literature could be a cause of the membranes drying out. Otherwise the lower A is caused by bad fitting of model, i.e. some of the concentration polarization being fitted as a lower permeability instead of mass transfer coefficients. However, the obtained parameters do to some extent fit the solutions. The best fits are obtained using the calculated osmotic pressures of the solutions instead of the measured osmotic pressures, probably due to experimental inaccuracy.
Model A has lower k_D than $k_{CP,F}$. This means, that the concentration polarization by feed dominates for this expression. On the contrary Model B has k_D is higher $k_{CP,F}$, giving a higher CP caused by draw than feed. Also, $k_{CP,F}$ for Model A is higher than for Model B, confirming that the ICP by NaCl could be higher than expected at 0-0.75 % NaCl. Though, k_D for Model B ,1-3.5 % NaCl, is also lower than k_D from Model A. Coupled with the fact, that the water permeability is lower than the values given in the literature, it is concluded that the fitted parameters does not represent the nature of the solutions, but just, to some extent, randomly fits the data. The bad fitting of data can be enhanced by the eventual concentration dependency of k_D, indicated from the experiment with 40 % PPG 425.
As the osmotic pressure depends on temperature, the flux can be modeled partly as a function of temperature. Though, k_D and $k_{CP,F}$ might also depend on temperature, as diffusion coefficients and viscosity vary with temperature. The viscosity's temperature dependence of 50 % PPG 425, given in figure 4.14 on page 49, show that the temperature increases with lower temperature. This will give a thicker boundary layer and lower diffusion coefficient and the ECP of the draw solution will increase. Therefore, the gain in osmotic pressure of draw for lowering the temperature to 10 ^{o}C has to be set up against the extra concentration polarization.
The filtrations modeled compared to experimental filtrations of 3.5 % NaCl with 60 %

PPG 425 and 0.4 % NaCl with 50 % PPG show higher modeled fluxes than experimental fluxes. This indicates a certain degree of fouling. How much fouling is unclear because of modeling uncertainties. The rejection of the 0.4 % NaCl with 50 % PPG experiment lasting 20 hours proved good, over 99 %. Though, this does not give a complete description of the rejection as it depends on the filtrate volume and flux. Instead it verifies that the transport over the membrane is water transport. Similar, the 0.4 % NaCl solution filtrated with 50 % PPG showed no presence of PPG from the draw solution.

Efficiency of Separation The separation with centrifugation showed a turbid sample in the start. After 20 minutes at 500 rpm and 55 ^{o}C, the sample starts to separate, as the upper part of the tubes shows more transmission of light. This indicates, that the upper phase, water phase because of lower density, contain fewer polymers. After 28 minutes, the lower phase also shows more transmission indicating, that the PPG phase release water. The two phases are separated by a decrease in transmission, indicating the boundary layer.

The characterization of the water phases from separation of PPG solutions has an error as a decrease in signal disturbed the signals from PPG polymers. Therefore only two peaks area per spectrum can be detected, and the overall concentration of PPG 425 is not determined. Nevertheless, the decrease in concentration of the first to peaks is detected. As the smallest PPG polymers are the most hydrophilic, these have least affinity to the C18 column, and will be detected first.

From the MS spectra in figure 4.17 on page 52 and 4.18 on page 52 it is observed, that there are detected higher molecular weight PPGs in the 50 % PPG 425 sample than in the water phases of separated solutions. This is a cause of the longer PPG's being least soluble, and precipitating first. This effects the average molecular weights estimated from the mass spectra. These are lower for the separated solutions than for the solution.

The average molecular weight of the water phase from the centrifuged sample is estimated to be roughly the same as the water phase from the precipitated sample. Neither the decrease in concentration of the first two peaks in HPLC shows a distinct difference between the two procedures for separation.

Higher temperature shows a more effective separation. Higher temperature causes more polymers to precipitate. The concentration decreases with about 60 % for peak 1 and 74 % for peak 2. Time does not show better separation after 2 hours than after 1 hour. Though, the separation at 60 ^{o}C after 2 hours show less separation than after 1 hour. This can be an error, caused by bad sampling after the separation. The lower decrease in concentration of peak 1 than peak 2 also demonstrates the effect of the shortest PPG's precipitating last.

To summarize, the osmotic pressure of PPG 425 solutions has been described by the van't Hoff equation for varying temperature and concentration.
Fluxes were obtained using PPG 425 draw and NaCl feed, but with a lower performance ratio than found in literature for other draw solutions. This is due to higher concentration polarization by the draw solution. The flux was modeled as a function of feed and draw osmotic pressures and concentration polarization.
The separation is ineffective, as there were still polymers left in the solutions after separation at 80 ^{o}C. This is caused by the polydispersity of the samples, as the shortest PPG's present does not precipitate. The high amount of polymer left after precipitation complicates further purification. This could be RO, but the high presence of PPG might give fouling. It is expected that the separation can be improved by using a monodisperse solution of PPG 425.
The usefulness of FO with PPG 425 draw depends on how effective the separation can be. Compared to the Ammonia carbonate system, the fluxes are low. Though, there is an advantage, that the PPG draw solution is not damaging the membrane, as the ammonia carbonate draw.
Further experiments of interest are to understand the high performance ratio of 40 % PPG 425. Is it linked to lower concentration polarization from PPG or is it just an error? Will a monodisperse PPG 425 solution give better separations than those obtained in this project, making PPG useful for draw solution?

6. Conclusion

The osmotic pressure of Polypropylene Glycol 425 solutions was described by the van't Hoff equation as dependent on both temperature and concentration. From this, the solutions is determined to have highest osmotic pressures at 15 ^{o}C of the temperatures investigated. At this temperature Polypropylene Glycol 425 create a flux from sodium chloride solutions. The flux is inhibited by concentration polarization, with a performance ratio of 3 to 6 %. For desalination of seawater 50 % Polypropylene Glycol 425 created a flux of water at 0.83 $\frac{L}{h \cdot m^2}$ from a 3.5 % sodium chloride solution, corresponding to sea water. The flux has been modeled, but the parameters does not show consistency with the values from literature.

At about 50 ^{o}C, Polypropylene Glycol 425 solutions of 20 to 60 % separated. Though, the separation of the solutions was ineffective. This is most likely caused by the polydispersity of the solutions, resulting in shorter chained polymers not separating. It is expected, that a monodisperse solution of Polypropylene Glycol 425 would give a more effective separation.

As it is not known, how to obtain complete regeneration of the Polypropylene Glycol 425 draw solution, and thereby reclaim fresh water from the solution, the efficiency and application of the draw solution has not been evaluated.

7. Nomenclature

Table 7.1: Overview of the nomenclature in this Thesis

a_s	Solute activity
a_w	Water activity
A	Water Permeability Constant
B	Second virial coefficient
B'	Second virial coefficient
c	Concentration
c_{bulk}	Concentration in bulk
c_D	Concentration of draw
c_F	Concentration of the solute in feed
c_{layer}	Concentration of solute in the layer
$c_{membrane}$	Concentration of solute in membrane
c_{NaCl}	Concentration of NaCl
c_P	Concentration of feed in permeate
c_s	Concentration of solute
C	Third virial coefficient
d_h	Hydraulic diameter
$\frac{dc}{dx}$	Concentration gradient within the boundary layer
D	Diffusion coefficient
F	Parameter dependent on q
G	Parameter dependent on I and q
h	Height relative to osmotic pressure difference between two solutions
I	Ionic Strenth
j	Constant related to the excess enthalpy
J_w	Flux of water
$J_{w,experimental}$	Experimental flux of water
$J_{w,theoretical}$	Theoretical flux of water
k	Mass transfer coefficient
k_D	Mass transfer coefficient for ECP in draw
k_F	Mass transfer coefficient for ECP in Feed
$k_{CP,F}$	k_F/K
K	Solute resistance to diffusion in support layer
m_s	mass of solute
M_s	Molar mass of solute

Continued on next page

Table 7.1 – continued from previous page

n	amount of substance
n_s	amount of solute
n_w	amount of water
p	Pressure
p_w	Water vapor pressure
p_w°	Water vapor pressure
p_w^T	Water vapor pressure at temperature T
$p_w^{T\circ}$	Water vapor pressure at dew point
P	External atmospheric pressure
q	Kusik-Meissner parameter
$r_{performance}$	Performance ratio
$r_{rejection}$	Rejection
R	Gas constant
Sh	Sherwood number
t	Thickness of support layer
T	Temperature
T_{ref}	Reference temperature
T°	Dew point temperature
V	Volume
$\overline{V}_w$	Partial molar volume of water
x_s	mole fraction of solute
x_w	mole fraction of water
Y	Water content
Y_{mono}	Water content at the surface of the adsorbing layer
Z_+	Charge of positive ions in electrolyte solution
Z_-	Charge of negative ions in electrolyte solution
Greek letters	
$\gamma_\pm$	Activity coefficient
ϵ	Porosity of the support layer
δ	Layer thickness
ΔC_p°	Difference in standard Heat Capacity
$\Delta C_{p,excess}^\circ$	Excess standard Heat Capacity
ΔG°	Difference in standard free Gibb's energy
ΔH°	Difference in standard Enthalpy
$\Delta H_{adsorption}^\circ$	Standard Adsorption Enthalpy
ΔH_{excess}°	Excess Standard Enthalpy

Continued on next page

Table 7.1 – continued from previous page

ΔH°_{vap}	Standard Vaporization Enthalpy
ΔS°	Difference in standard Entropy
$\Delta S^{\circ}_{adsorption}$	Standard Adsorption Entropy
$\Delta S^{\circ}_{excess}$	Excess standard Entropy
ΔP	Difference in applied pressure
$\Delta \mu_w$	Difference in chemical potential of water
$\left(\frac{\Delta \mu_w}{\Delta P}\right)_T$	Difference in chemical potential of water with varying pressure and constant T
$\Delta \Pi$	Difference in osmotic pressure of two solutions
μ_w	Chemical potential of water
μ°_w	Standard chemical potential of water
Π	Osmotic pressure
Π_{bulk}	Osmotic pressure in bulk
Π_D	Osmotic pressure of Draw solution
Π_F	Osmotic pressure of Feed solution
$\Pi_{membrane}$	Osmotic pressure at the membrane
τ	Tortuosity of the support layer

Bibliography

[Atkins and de Paula, 2002] Atkins, P. and de Paula, J. (2002). *Atkins' Physical Chemistry*. Oxford University Press, seventh edition.

[Batchelder, 1965] Batchelder, G. W. (1965). Process for the demineralization of water. *US Patent 3,171,799*.

[Bixio et al., 2006] Bixio, D., Thoeye, C., de Koning, J., Joksimovic, D., Savic, D., Wintgens, T., and Melin, T. (2006). Wastewater reuse in europe. *Desalination*, 187:89–101.

[Cath et al., 2006] Cath, T. Y., Childress, A. E., and Elimelech, M. (2006). Forward osmosis: Principles, applications, and recent developments. *Journal of Membrane Science*, 281:70–87.

[Cath et al., 2005] Cath, T. Y., Gormly, S., Beaudry, E. G., Flynn, M. T., Adams, V. D., and Childress, A. E. (2005). Membrane contactor processes for wastewater reclamation in space part i. direct osmotic concentration as pretreatment for reverse osmosis. *Journal of Membrane Science*, 257:85–98.

[Clement et al., 2004] Clement, K. H., Fangel, P., Jensen, A. D., and Thomsen, K. (2004). *Kemiske Enhedsoperationer*. Polyteknisk Forlag, fifth edition.

[Devagon Devices, udat] Devagon Devices, U. (udat.). *Operator's Manual Aqua Lab 4 Water Activity Meter*.

[Frank, 1972] Frank, B. S. (1972). Desalination of seawater. US Patent 3,670,897.

[Glew, 1965] Glew, D. N. (1965). Process for liquid recovery and solution concentration. *US Patent 3,216,930*.

[Gray et al., 2006] Gray, G. T., McCutcheon, J. R., and Elimelech, M. (2006). Internal concentration polarization in forward osmosis: role of membrane orientation. *Desalination*, 197(3):1–8.

[Hiemenz and Rajagopalan, 1997] Hiemenz, P. and Rajagopalan, R. (1997). *Principles of Colloid and Surface Chemistry*. Marcel Dekker, Inc., third edition. PP 105-144.

[Holloway et al., 2007] Holloway, R. W., Childress, A. E., Dennett, K. E., and Cath, T. Y. (2007). Forward osmosis for concentration of anaerobic digester centrate. *Water Research*, 41:4005–4014.

[Hvidt, 2007] Hvidt, S. (2007). Viscosity of peg 2000.

[Kirk, 1966] Kirk, R. E. (1966). *Encyclopedia of Chemical Technology.* second edition. Volume 10.

[Kravath and Davis, 1975] Kravath, R. and Davis, J. (1975). Desalination of seawater by direct osmosis. *Desalination*, 16:151–155.

[Lee et al., 1981] Lee, K. L., Baker, R. W., and Lonsdale, H. K. (1981). Membranes for power generation by pressure-retarded osmosis. *Journal of Membrane Science*, 8:141–171.

[Malcolm and Rowlinson, 1957] Malcolm, G. N. and Rowlinson, J. S. (1957). The thermodynamic properties of aqueous solutions of polyethylene glycol, polypropylene glycol and dioxane. *Transactions of the Faraday Society*, 53:921–931.

[McCutcheon and Elimelech, 2006] McCutcheon, J. R. and Elimelech, M. (2006). Influence of concentrative and dilutive internal concentration polarization on flux behavior in forward osmosis. *Journal of Membrane Science*, 284:237–247.

[McCutcheon and Elimelech, 2007] McCutcheon, J. R. and Elimelech, M. (2007). Modeling water flux in forward osmosis: Implications for improved membrane design. *American Institute of Chemical Engineers Journal*, 53(7):1736–1744.

[McCutcheon et al., 2005] McCutcheon, J. R., McGinnis, R. L., and Elimelech, M. (2005). A novel ammonia-carbon dioxide forward (direct) osmosis desalination process. *Desalination*, 174:1–11.

[McCutcheon et al., 2006] McCutcheon, J. R., McGinnis, R. L., and Elimelech, M. (2006). Desalination by ammonia-carbon dioxide forward osmosis: Influence of draw and feed solution concentrations on process performance. *Journal of Membrane Science*, 278:114–123.

[McGinnis and Elimelech, 2007] McGinnis, R. L. and Elimelech, M. (2007). Energy requirements of ammonia-carbon dioxide forward osmosis desalination. *Desalination*, 207:370–382.

[Mi and Elimelech, 2008] Mi, B. and Elimelech, M. (2008). Chemical and physical aspects of organic fouling of forward osmosis membranes. *Journal of Membrane Science*, 320:292–302.

[Mulet et al., 1999] Mulet, A., Garcia-Reverter, J., Sanjuán, R., and Bon, J. (1999). Sorption isosteric heat determination by thermal analysis and sorption isotherms. *Journal of Food Science*, 64(1):64–68.

[Petrotos et al., 1999] Petrotos, K. B., Quantick, P. C., and Petropakis, H. (1999). A study of the direct osmotic concentration of tomato juice in tubular membrane - module

configuration. ii. the effect of certain basic process parameters on the process performance. *Journal of Membrane Science*, 160:171–177.

[Schiermeier, 2008] Schiermeier, Q. (2008). Purification with a pinch of salt. *Nature*, 452:260–261.

[Shannon et al., 2008] Shannon, M. A., Bohn, P. W., Elimelech, M., Georgiadis, J. G., Mariñas, B. J., and Mayes, A. M. (2008). Science and technology for water purification in the coming decades. *Nature*, 452:301–310.

[Weilby, 2008] Weilby, L. (2008). *Phase equilibrium of the Polypropylene Oxide - water system*. Roskilde University, Denmark. Ph.D. Dissertation.

[York et al., 1999] York, R. J., Thiel, R. S., and Beaudry, E. G. (1999). Full-scale experience of direct osmosis concentration applied to leachate management. Proceedings of the Seventh International Waste Management and Landfill Symposium (Sardinia 1999), S. Margherita di Pula, Cagliari, Sardinia, Italy.

A. Concentration and temperature dependence of osmotic pressure of NaCl solutions

To describe the osmotic pressure of NaCl solutions of different concentrations and temperature, the osmotic pressure of electrolyte solutions has to be expressed. From equation A.1 the osmotic pressure of electrolyte solutions can be expressed [Clement et al., 2004]:

$$\Pi = -\frac{iRT}{\bar{V}_w} ln(1 - a_s) \tag{A.1}$$

Where i is the number of electrolytes in solution. As $a_s = \gamma_{\pm} \cdot x_s$ the equation is extended:

$$\Pi = -\frac{iRT}{\bar{V}_w} ln(1 - \gamma_{\pm} \cdot x_s) \tag{A.2}$$

In this expression, the activity coefficient, $\gamma_{\pm}$, is temperature dependent. Cisternas and Galleguillos (1989) have determined the temperature dependence by the following expression:

$$Log(\gamma_{\pm}) = \left(-0.5107 \left|Z_+ Z_-\right| \sqrt{I}\right) / \left(1 + G\sqrt{I}\right) + \left|Z_+ Z_-\right| Log\left(1 + 0.5107 \left(1 + 0.1I\right)^q - F\right) \tag{A.3}$$

Where

F= $0.75 - 0.065q$

G= $0.055q exp\left(-0.023I^3\right)$

I= $\frac{1}{2} \sum_i c_i Z_i^2$

q is the temperature dependent Kusik-Meissner parameter and Z_+ and Z_- are the charges of the positive and negative ions respectively.
These parameters causes the activity coefficients temperature dependency. From the data given in Cisternas and Galleguillos (1989) the temperature dependency of q is plotted in figure A.1 on the facing page.

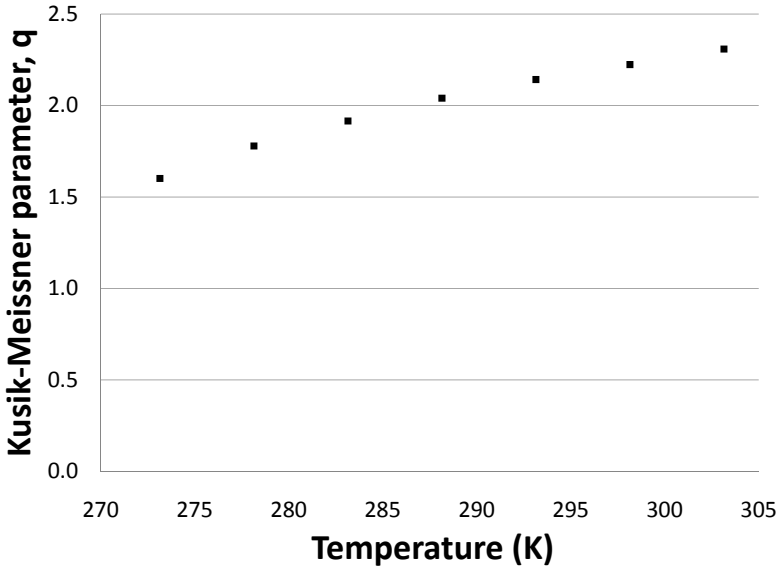

Figure A.1: Kusik-Meissner parameter, q, plotted against temperature. Data from Cisternas and Galleguillos (1989).

From the plot, q is fitted $q = 6.674ln\,(T) - 35.793$ with R^2=0.9841. Combining this fit with equation A.2 on the preceding page and A.3 on the facing page gives an expression of osmotic pressure of NaCl solutions as a function of temperature and concentration, given in equation vrefeq:sidste:

$$\Pi = 1.013(10.0171 \cdot c_{NaCl} - 0.0004) \cdot T + 1.8017 \cdot c_{NaCl} - 0.0509 \qquad \text{(A.4)}$$

Where c_{NaCl} is the concentration of NaCl in %.